



UNDERGRADUATE PROJECT REPORT

Project Title:	DIRA-Net on Breast Cancer Diagnosis
Surname:	Wu
First Name:	Albert
Student Number:	202018102012
Supervisor Name:	Dr Grace Ugochi Nneji
Module Code:	CHC 6096
Module Name:	Project
Date Submitted:	May 5, 2023

Chengdu University of Technology Oxford Brookes College

Chengdu University of Technology

BSc (Single Honours) Degree Project

Programme Name: Projects

Module No.: CHC 6096

Surname: Wu

First Name: Albert

Project Title: DIRA-Net on Breast Cancer Diagnosis

Student No.: 202018010212

Supervisor: Dr. Grace Ugochi Nneji

Date submitted: 6rd May 2024

*A report submitted as part of the requirements for the degree of BSc (Hons) in Computer
Science*

At

Chengdu University of Technology Oxford Brookes College

Declaration

Student Conduct Regulations:

Please ensure you are familiar with the regulations in relation to Academic Integrity. The University takes this issue very seriously and students have been expelled or had their degrees withheld for cheating in assessment. It is important that students having difficulties with their work should seek help from their tutors rather than be tempted to use unfair means to gain marks. Students should not risk losing their degree and undermining all the work they have done towards it. You are expected to have familiarised yourself with these regulations.

<https://www.brookes.ac.uk/regulations/current/appeals-complaints-and-conduct/c1-1/>

Guidance on the correct use of references can be found on www.brookes.ac.uk/services/library, and also in a handout in the Library.

The full regulations may be accessed online at
<https://www.brookes.ac.uk/students/sirt/student-conduct/>

If you do not understand what any of these terms mean, you should ask your Project Supervisor to clarify them for you.

I declare that I have read and understood Regulations C1.1.4 of the Regulations governing Academic Misconduct, and that the work I submit is fully in accordance with them.

Signature

Abserve. Keliang Wu.

Date6th May 2024.....

REGULATIONS GOVERNING THE DEPOSIT AND USE OF OXFORD BROOKES
UNIVERSITY MODULAR PROGRAMME PROJECTS AND DISSERTATIONS

Copies of projects/dissertations, submitted in fulfillment of Modular Programme requirements and achieving marks of 60% or above, shall normally be kept by the Oxford Brookes University Library.

I agree that this dissertation may be available for reading and photocopying in accordance with the Regulations governing the use of the Oxford Brookes University Library.

Signature



Date6th May 2024.....

Acknowledgment

In completing my project on the application of deep learning in breast cancer detection, I am immensely grateful for the guidance and support of Dr. Grace Ugochi Nneji, my supervisor, and Joojo Walker, my Module Leader. Dr. Grace provided valuable insights and rigorous supervision throughout the research process, greatly enhancing my work. Joojo Walker, while primarily responsible for delivering course content, also offered significant help that facilitated my understanding and application of complex concepts. Their combined support was crucial in the successful completion of my project. Thank you for your dedication and assistance.

Table of Contents

Declaration	i
Acknowledgment	iii
Table of Contents	iv
List of Figures	vii
List of Tables	xi
Abstract	xii
Abbreviations	xiii
Glossary	xv
Chapter 1 Introduction.....	1
1.1 Background	1
1.1.1 Convolution Neural Network Overview	2
1.1.2 Convolution Layer	3
1.1.3 Pooling Layers	5
1.1.4 Batch Normalization	5
1.1.5 Fully Connected Layers	6
1.1.6 Dropout Layers	6
1.1.7 Rectifier Linear Unit	6
1.1.8 Kernel intializer - He_Initialization	7
1.1.9 Loss Function	7
1.2 Aim	8
1.3 Objectives	8
1.4 Project Overview	9
1.4.1 Scope	9
1.4.2 Audience	9
Chapter 2 Background Review	11

Chapter 3 Methodology	14
3.1 Approach	14
3.1.1 Model Construction	14
3.1.1.1 Inception Network Version 4	14
3.1.1.2 Residual Network	16
3.1.1.3 Depthwise Convolution Model.....	16
3.1.1.4 Attention Mechanism	16
3.1.1.5 Inception-ResNet Model	17
3.1.1.6 Depthwise-Inception-ResNet Model	18
3.1.1.7 Depthwise-Inception-ResNet-Attention Model	19
3.1.1.8 The Proposed Model	19
3.2 Dataset.....	20
3.2.1 Dataset Introduction	20
3.2.2 Data Separation	21
3.2.3 Data Balance	22
3.2.4 Data Resize	23
3.2.5 Data Color Channel Modification	23
3.2.6 Data Augmentation	24
3.2.7 Data Preprocessing Summary	24
3.3 Technology	24
3.4 Data Testing and Evaluation Plan	25
3.4.1 Data Testing	25
3.4.2 Model Performance Evaluation Criteria	26
Chapter 4 Experiment and Results	28
4.1 Experiment Phases	28
4.2 Inception-Net Training on Four Magnification	28

4.3 ResNet Training on Four Magnification	34
4.4 Depthwise Network Training on 40X Magnification	37
4.5 Inception-ResNet (IR-Net) Training on 40X Magnification	38
4.6 Depthwise-Inception-ResNet (DIR-Net) Training on 40X Magnification	40
4.7 DIRA-Net Training on 40X Magnification	42
4.8 CLAHE Experiment.....	43
4.9 Model Evolution Summary	43
4.10 Fine Tune	44
4.11 Comparison Analysis	54
4.12 Model Visualization	56
4.13 Model Deployment.....	57
Chapter 5 Project Management.....	60
5.1 Activities	60
5.1.1 Schedule	61
5.1.2 Project Version Management	61
5.1.3 Project Data Management	62
5.1.4 Project Deliverable	62
5.2 Risk Analysis	62
5.3 Professional Issues	63
Chapter 6 Conclusion	65
Reference	66
Appendices	71

List of Figures

Figure 1 : Convolutional Neural Network Overview	3
Figure 2 : Convolutional Layer and Calculation	4
Figure 3 : Sliding operation of filters	4
Figure 4 : Two types of Padding Methods	5
Figure 5 : Two types of Pooling Layers.	5
Figure 6 : ReLU and Leaky ReLU Graph	7
Figure 7 : Inception V4 Architecture	14
Figure 8 : InceptionV4 STEM Block	14
Figure 9 : Detail Blocks within InceptionV4.	15
Figure 10 : Basic ResNet Block	16
Figure 11 : Depthwise Convolution	16
Figure 12 : Attention Block	17
Figure 13 : Inception-ResNet-Prototype	17
Figure 14 : STEM Block of Inception-ResNet Protoype Model	17
Figure 15 : Detail structure of Inception-ResNet model	18
Figure 16 : Depthwise-Inception-ResNet Model	19
Figure 17 : Depthwise-Inception-ResNet STEM block with attention mechanism ...	19
Figure 18 : The proposed model DIRA-Net	20
Figure 19 : Examples of BreakHis Images	21
Figure 20 : Dataset Structure after Separation	22
Figure 21 : Number of images within Benign and Malignant Before Balancing	22
Figure 22 : Images Number After Balancing	23
Figure 23 : Images Transformation	23

Figure 24 : Augmented image example	24
Figure 25 : Initial Inception Model for experiment	28
Figure 26 : Inception-Net Accuracy and Loss on 40X Raw Images	29
Figure 27 : Inception-Net Accuracy and Loss on 100X Raw Images	29
Figure 28 : Inception-Net Accuracy and Loss on 200X Raw Images	30
Figure 29 : Inception-Net Accuracy and Loss on 400X Raw Images	30
Figure 30 : Inception-Net Accuracy and Loss on 40X Resize Images	31
Figure 31 : Inception-Net Accuracy and Loss on 100X Resize Images	31
Figure 32 : Inception-Net Accuracy and Loss on 200X Resize Images	32
Figure 33 : Inception-Net Accuracy and Loss on 400X Resize Images	32
Figure 34 : Inception-Net Comparison Accuracy	33
Figure 35 : Inception-Net Comparison of Validation Loss	33
Figure 36 : Initial ResNet Structure for experiment	34
Figure 37 : ResNet Accuracy and Loss on 40X Resized Images	34
Figure 38 :ResNet Accuracy and Loss on 100X Resized Images	35
Figure 39 : ResNet Accuracy and Loss on 200X Resized Images	35
Figure 40 : ResNet Accuracy and Loss on 400X Resized Images	36
Figure 41 : ResNet Validation Accuracy Comparison	37
Figure 42 : ResNet Validation Loss Comparison	37
Figure 43 : Depthwise CNN for experiment	38
Figure 44 : Depthwise-CNN Accuracy and Loss on 40X Magnified Images	38
Figure 45 : Inception-ResNet STEM block	39
Figure 46 : Inception-ResNet Structure for experiment	40
Figure 47 : InceptionResNet Accuracy and Loss on 40X Resized Images	40

Figure 48 : Depthwise-Inception-ResNet Block A	41
Figure 49 : DIR model overview.	41
Figure 50 : DIR-Net Accuracy and Loss on 40X Magnified Images	41
Figure 51 : STEM Block with attention mechanism	42
Figure 52 : Initial DIRA-Net.....	42
Figure 53 : Initial DIRA-Net accuracy and loss	43
Figure 54 : CLAHE Test Results	43
Figure 55 : DIRA-Net Fine-tune result 1	46
Figure 56 : DIRA-Net Fine-tune result 2	47
Figure 57 : DIRA-Net Fine-tune result 3	47
Figure 58 : DIRA-Net Fine-tune result 4	48
Figure 59 : DIRA-Net Fine-tune result 5	49
Figure 60 : DIRA-Net Fine-tune result 6	49
Figure 61 : DIRA-Net Fine-tune result 7	50
Figure 62 : DIRA-Net Fine-tune result 8	50
Figure 63 : DIRA-Net Fine-tune result 9 (Proposed One)	51
Figure 64 : DIRA-Net evaluation metrix	53
Figure 65 : DIRA-Net Validation Accuracy Comparison with Pre-trained Models	55
Figure 66 : DIRA-Net Validation Loss Comparison with Pre-trained Models	56
Figure 67 : SHAP Visualization	57
Figure 68 : Grad-CAM Visualization	57
Figure 69 : Main Page	58
Figure 70 : Dataset Introduction Cards	58
Figure 71 : Diagnosis Page before Diagnosis	59

Figure 72 : Malignant Diagnosis 59

Figure 73 : Benign Diagnosis 59

List of Tables

Table 1 : Summary of Related Works	1
Table 2 : Upsampling detail for each magnification	24
Table 3 : Different Augmentation of Different Magnification	24
Table 4 : Summary of Relevant Technology involved in this project	25
Table 5 : Model Evolution Summary	44
Table 6 : Hyperparameters of the initial DIRA-Net	45
Table 7 : Hyperparameters of model fine tune version 1	45
Table 8 : Hyperparameters of version 2	46
Table 9 : Hyperparameters for version 3	47
Table 10 : Hyperparameters of Version 4	48
Table 11 : Hyperparameters of Version 5	48
Table 12 : Hyperparameters of Version 6	49
Table 13 : Hyperparameters of Version 7	49
Table 14 : Hyperparameters of Version 8	50
Table 15 : Hyperparameter of Proposed Version	51
Table 16 : Fine tune process and results summary	54
Table 17 : Comparison Analysis with Previous Works	55
Table 18 : Results Comparison of DIRA-Net with Pre-trained Models	56
Table 19 : Activities of the Project	60
Table 20 : Gantt Graph	61
Table 21 : Version Control Progress	62
Table 22 : Risk Analysis	63

Abstract

Breast Cancer ranks among the deadliest diseases globally, posing significant diagnostic challenges that demand the expertise of radiologist, state-of-art equipment, and considerable resources. Traditional diagnostic methods have struggled with accuracy, leading to misdiagnosis. Although advancements in medical image processing have improved outcomes, inaccuracies in breast cancer diagnosis remain a critical issue. This project leverages deep learning to enhance diagnostic precision through the development of a novel convolutional neural network (CNN) model, termed the Depthwise-Inception-ResNet, incorporating an attention mechanism. This innovative model combines the strengths of the Inception and Residual networks with attention block, enabling it to focus on granular features while maintaining sufficient depth to extract critical feature for accurate breast cancer classification. Trained and validated on histopathological images from public BreakHis dataset, the model achieved remarkable performance metrics: 96.45% accuracy, 93% AUC, and 92.14% F1-Score. These results underscore the model's efficacy in the nuanced classification of breast cancer, heralding a significant advancement in diagnostic methodologies.

Keywords: *CNN, Breast Cancer, Deep Learning, Inception-Net, ResNet, Depthwise-Net, Attention Mechanism*

Abbreviations

CNN	Convolutional Neural Network
ResNet	Residual Network
GAP	Global Average Pooling
TP	True Positive
TN	True Negative
FP	False Positive
FN	False Negative
ReLU	Rectified Linear Unit
IR-Net	Inception Residual Network
DIR-Net	Depthwise Inception Residual Network
DIRA-Net	Depthwise Inception Residual Attention Network
Acc	Accuracy
Prec	Precision
Spec	Specificity
Para	Parameters
F1	F1-Score
Rec	Recall
AUC	Area Under Curve
CLAHE	Contrast Limited Adaptive Histogram Equalization
MRI	Magnetic Resonance Imaging
RR	Rotation Range
WS	Width Shift
HS	Height Shift
SR	Shear Range
ZR	Zoom Range
HF	Horizontal Flip
FM	Fill Mode

LR	Learning Rate
VN	Version Number
BS	Batch Size
L2	L2 Regularization
FN	First Three Layers Filter Number of STEM Block

Glossary

Convolutional Neural Network: An architecture of network utilized for deep learning mission which are commonly used for computer vision projects

Residual Network: A deep learning architecture that uses skip connections to prevent gradient issues in very deep networks.

Inception-V4: An advanced deep learning model that enhances the Inception architecture with more complex and efficient structures to improve accuracy and speed.

Depthwise Convolution: A convolutional operation that separates the filtering and combining steps, allowing for reduced computational cost and model size in deep neural networks.

Data Augmentation: A technique used to increase the diversity of data available for training models by applying random transformations to training images.

Data Separation: The process of dividing data into distinct sets, typically for training, validation, and testing purposes.

Data Balance: The concept of ensuring that each class in a dataset is equally represented to prevent model bias and improve generalization across different categories.

Color Channel Modification: Adjusting the intensity values of the color channels in an image to alter its appearance or to perform normalization.

Resize: Changing the dimensions of an image, often to meet the input size requirements of a neural network.

Pre-trained Model: A model that has been previously trained on a large dataset and can be fine-tuned or used directly for similar tasks.

Fine tune: The process of adjusting the parameters of a pre-trained model to make it more suitable for a specific, often related task.

Chapter 1 Introduction

1.1 Background

Breast Cancer is one of the most fatal diseases so far in the world. It is said by American Cancer Society Surveillance that one of eight women is affected by it [1]. According to statistics recorded by the World Health Organization (WHO) [2] among the 9.6 million cancer-related deaths, 627,000 females passed away due to breast cancer in 2018, in addition, WHO had also predicted that 43, 600 women would die from breast cancer in 2021 [3], which indicates that breast cancer remains the leading cause of women deaths.

Breast cancer is similar to other types of cancer which has early-stage (Benign) and later-stage (Malignant). Once the disease reaches the malignant stage, cancer might spread to other parts of the body which leads to catastrophic consequences, therefore, it is crucial to detect breast cancer at the early stage in order to provide appropriate treatment [4]. Mammography serves as a common approach for breast cancer detection in which the picture is normally taken through Magnetic Resonance Imaging (MRI), X-Ray, and Ultrasound, and a study had confirmed that these images raised survival rate [5]-[6]. Another method which is also widely used is biopsy. It relies on tissue samples from the cancer area of breasts and complete the analysis, classification, and detection under the microscope [5]. Furthermore, breast cancer were also analyzed on cytological level [7].

However it is unfortunate that the diagnosis still faces troubles even with numerous methods applied for correctly diagnosing the area of breast cancer and classifying the category in medical image processing [8]. Manual diagnosis through medical images or microscope is time-intensive, expensive and prone to errors, as symptoms are likely to be overseen [9]. For example, ultrasound breast image detection highly depends on the experience, capability and knowledge of radiologists and diagnosticians [10], which most likely to be an issue with the lack of facilities, resources, and manpower in small hospitals.

Recent years, with the rapid evolution of deep learning in medical image processing,

the application of Computer-Aided-Diagnosis has been widely acknowledged [5]. As the demand for accuracy and speed in breast cancer image analysis continues to increase, the application of deep learning technology has become a major trend in this field [11].

Within the realm of breast cancer research, CNNs stand as a pivotal element, particularly in the classification and diagnosis of the disease. CNNs are renowned not only for their precision in feature extraction and accurate classification but also for their capability in managing image pattern matching tasks within extensive datasets [5]. These networks excel in processing a vast array of medical images, including mammograms, ultrasound, MRI, and histopathological images, to differentiate between benign and malignant lesions effectively. The primary aim of this project is to harness the power of CNNs through the development and deployment of a deep-learning-based system dedicated to the classification and diagnosis of breast cancer. This initiative seeks to reduce the reliance on manual diagnostic efforts, target treatments more precisely, decrease mortality rates, and ultimately save lives by enhancing the accuracy and efficiency of breast cancer detection. The integration of CNNs into this project underscores their critical role in advancing diagnostic methodologies, ensuring optimal resource utilization, and improving patient care outcomes.

1.1.1 Convolution Neural Network Overview

Before getting into the detailed of this project, the following part will introduce the knowledge of CNNs and the specific techniques within the project. The basic concept includes convolution, pooling, activation function, loss function, batch normalization, etc.

CNNs are sophisticated models comprising three primary types of layers: the input layer, hidden layers, and the output layer. The essence of a CNN lies within its hidden layers, which dictates the model's structure through a series of convolutional layers, pooling layers, activation functions, and padding, among other components. These layers work collectively to downsample and process image data, a technique crucial

for reducing complexity while retaining significant information [12].

Upon entry into a CNN, an image is defined by its height, width, and depth—the latter representing color channels. It then undergoes a sequential transformation through various layers, each performing mathematical operations to extract features and reduce dimension. This process includes the application of non-linearity to interpret the image's content, leading to predictions or classifications. Through this intricate sequence of transformations, known as convolution, the network leverages learned patterns to efficiently analyze images. The original high-dimensional input is methodically condensed into a form that emphasizes essential information, facilitating effective output. This streamlined overview of CNNs illustrates their capacity to interpret and classify images, highlighting the role of their hierarchical structure in image processing. Figure 1 depicts an overview of the CNN structure, including its processes.

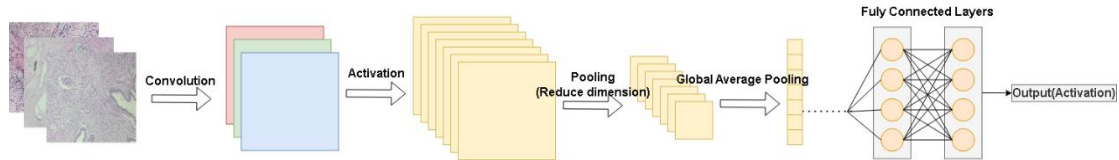
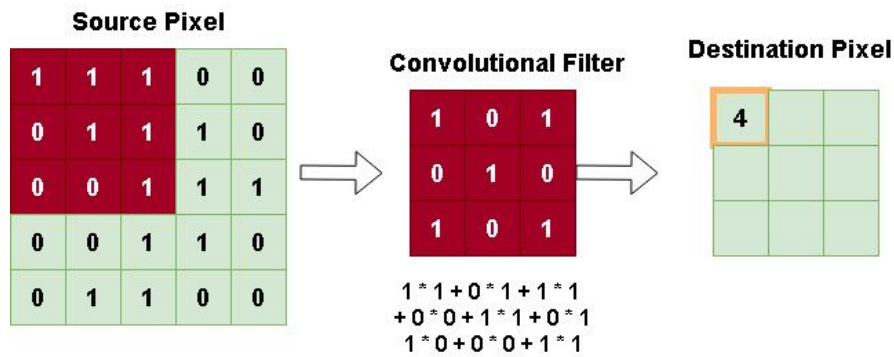


Figure 1: Convolutional Neural Network Overview

1.1.2 Convolution Layer

Convolutional layers perform features extraction with convolution operations. The operation is complete by using filters set with size and strides which varies from model to model. Filters are matrix used to detect specific types of features by performing element-wise multiplications followed by a sum wherever it is slide through in order to produce an output feature map [13]. This feature map indicates the presence and intensity of those features across the image. Note that adjusting the filter size, stride, and padding affects how the layer captures and scale these features, enabling the network to learn complex patterns and structures from visual data effectively. The construction process of a typical convolutional layer is depicted in Figure 2.



Red Part is where the filter is overlay representing where filter is scanning

Figure 2: Convolutional Layer and Calculation

Stride determines the movement of filters across the input, and padding allows for adjustment of the input's spatial dimensions to preserve edge information in the output. Each affects spatial dimensions and theoretical integrity respectively. Figure 3 displays the sliding of filters and the padding operation.

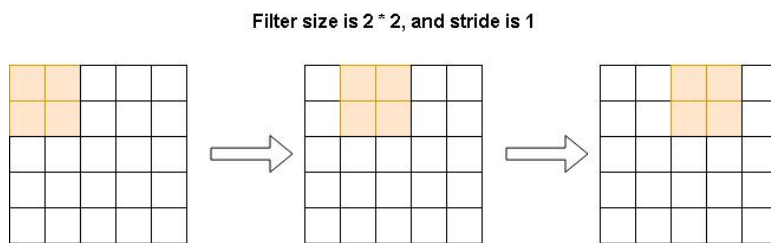
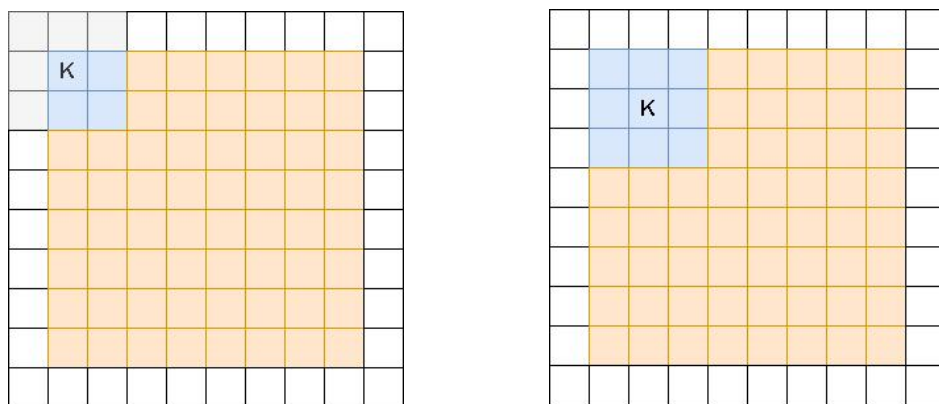


Figure 3: Sliding operation of filters

There are two patterns of padding in this project, "Same" and "Valid". "Same" pattern only starts calculating when the center of the filters overlap with the input image whereas valid starts calculating only when the full size of filter has entered the input image area. Figure 4 illustrates the padding mode.



a) Padding of mode “same”

b) Padding of mode “valid”

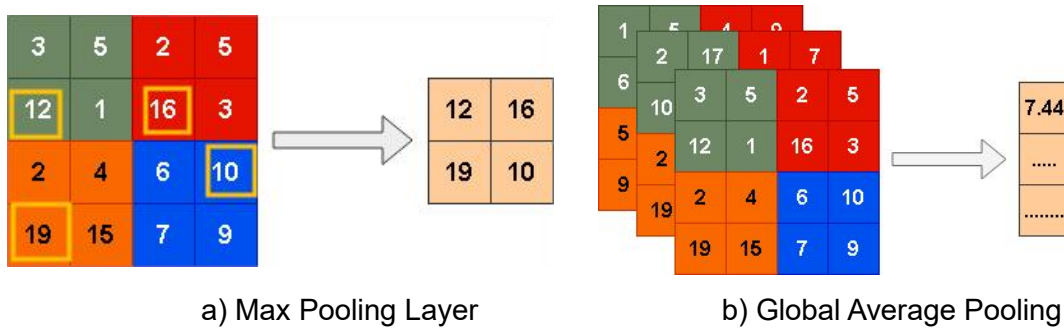
Figure 4: a) and b) illustrates two padding modes which is frequently used in this project. K represents the center of the kernel, Gray area display the full size of the filter, blue area is the overlapping area of filter and input images.

1.1.3 Pooling Layers

Pooling layers simplify the information in feature maps by summarizing the presence of features in patches of the feature map. Two of the pooling layers are frequently used in the project, Max Pooling and Global Average Pooling.

Max Pooling picks the largest value from each patch of the feature map, preserving the most prominent features while reducing dimensionality.

Global Average Pooling calculates the average of all values in each feature map, condensing each map to a single value. This helps reducing the complexity of model and aids classification tasks by focusing on the overall presence of features across the map. Overview how both pooling layers function is in Figure 5.



a) Max Pooling Layer

b) Global Average Pooling

Figure 5: a) and b) represents two pooling layers where a) is operated under a pooling filter of $2 * 2$, which selects the biggest number in each zone. GAP on the other hand calculates the mean average of each channel get the output.

1.1.4 Batch Normalization

Batch normalization (BN) is a technique widely used in deep learning to normalize the inputs of each layer. It helps in stabilizing and speeding up the training process [14].

The basic equation is in Equation (1).

$$BN(x) = \gamma \frac{x - \mu_B}{\sqrt{\sigma_B^2 + \epsilon}} + \beta \quad \text{Equation (1)}$$

X represents the input, μ_B is the mean of the batch, σ_B^2 is the variance of the batch,

ϵ is the small constant added for numerical stability, and γ and β are learnable parameters for scale and shift, respectively.

1.1.5 Fully Connected Layers

Fully connected (dense) layers integrate and summarize features extracted by previous layers to make predictions. Each neuron connects to every neuron in the preceding layer, enabling the model to consider all learned features for tasks like classification or regression. Positioned after convolutional and pooling layers, they translate complex feature representations into outcomes.

1.1.6 Dropout Layers

Dropout serves as a regularization technique in neural networks to prevent overfitting. It operates by randomly setting a fraction of neurons into zero within each update during training which effectively shrinks the network temporarily. The dropout rate is typically defined as hyperparameter “p”, representing the probability of neuron being dropped. Dropout operation is not applied during testing, however, neuron outputs are scaled by “p” therefore maintaining the consistency of the overall network.

1.1.7 Rectifier Linear Unit

Non-linearity is introduced through activation functions like ReLU(Rectified Linear Unit), is crucial in neural networks to enable the modeling of complex patterns.

ReLU and Leaky ReLU are popular activation functions in deep neural networks, particularly effective in addressing non-linear problems.

ReLU activation possesses a quicker convergence rate and calculation speed due to its linear operation, and Leaky ReLU function with leak correction variants from the classical ReLU activation resolves the issue of ReLU might cause neuron deaths when the input value is negative[15]. The function graph and equation is illustrated in Figure 6 and Equation (2) to Equation (3).

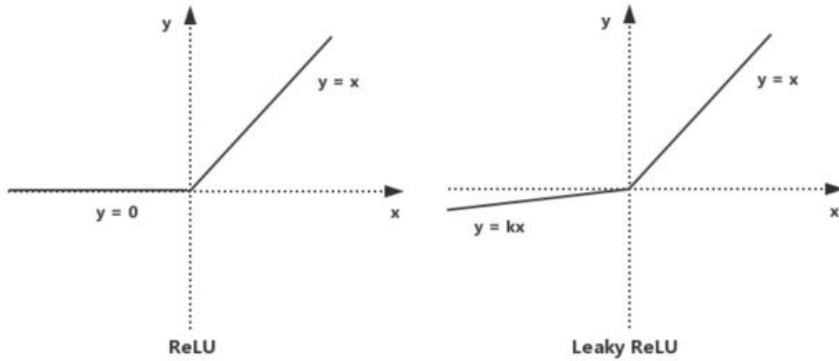


Figure 6: ReLU and Leaky ReLU function graph, where k is fixed for Leaky ReLU

$$\text{Leaky-ReLU } (x) = \max(kx, x) = \begin{cases} x, & \text{if } x > 0 \\ kx, & \text{if } x \leq 0 \end{cases} \quad \text{Equation (2)}$$

$$\text{ReLU } (x) = \max(kx, x) = \begin{cases} x, & \text{if } x > 0 \text{ (Activate State)} \\ 0, & \text{if } x \leq 0 \text{ (Inactivate State)} \end{cases} \quad \text{Equation (3)}$$

1.1.8 Kernel initializer - He_Initialization

According to He et al., [16], introduces an initialization method that is particularly effective for layers using rectifier activation(ReLU or its deviations) functions. This method, commonly known as “He_Initialization”. This concept was built to address the problem of gradient vanish and exploding which frequently appears in deep neural networks.

He_Initialization sets the initial network weights close to zero but scaled by $\sqrt{2/n}$, ensuring stable gradients and faster convergence of the model equation is provided in Equation (4).

$$W \sim N(0, \sqrt{2/n}) \quad \text{Equation (4)}$$

W is the weight matrix for ta layer in the neural network, $N(0, \sqrt{2/n})$ displays the normal (Gaussian) distribution with mean 0 and standard deviation. n represents the number of incoming connections (fan-in) to the layer. The biases are normally initialized to 0.

1.1.9 Loss Function

Loss function measures the difference between the model’s predictions and the actual data, acting as the objective for optimization; the measurement is essential for

guiding the network through the learning process, enabling it to accurately interpret input data. By minimizing the loss function, the network adjusts its internal parameters to improve prediction accuracy, serving as the foundational mechanism for the model's adaptation and refinement [14].

1.2 Aim

Various models in deep learning diagnosis utilize a specific single model or single mechanism, however, by doing so, there are chances that flaws of specific models could affect the performance in a negative way. To eliminate the drawbacks and maximize the performance, this project aims to develop and deploy a novel CNN model including Inception-ResNet mechanism to classify the levels of breast cancer. Based on Wang et al. [17], Inception-ResNet possesses a remarkable balance between model accuracy and resource efficiency.

1.3 Objectives

The project will collect breast cancer symptom data from online sources, utilizing public datasets BreakHis. BreakHis has benign and malignant categories with 9,109 microscope images from 82 patients. The data will be divided into training and testing sets for four different scaled images, with an 75% portion allocated for training and a 15% portion for testing. Within the training set, 15% of the images will be randomly selected as a validation set. It is essential to include both benign and malignant samples in both sets.

The project aims to build a Depthwise-Inception-ResNet-Attention model, with hyperparameter adjustments such as batch size, learning rate, dropout rate etc. Although primarily focused on binary classification, the project also approaches it as a multi-class problem which facilitates future generalization on detail symptoms.

In addition, the evaluation of the model will include metrics such as "Accuracy" and "Loss." Moreover, performance will be assessed using "Precision", "Recall", "F1-Score", "AUC-ROC", "AUC-PR", "Specificity", "Sensitivity", and the "Confusion Matrix".

Lastly, the project will be deployed through a website which allows uploading medical

pictures of breast cancer, and then give the classification results.

1.4 Project Overview

This section explores the potential of Inception-ResNet for improving breast cancer diagnosis, highlighting key stakeholders who will benefit from these advancements in medical image processing.

1.4.1 Scope

CNNs were introduced to medical image processing in the 1980s and have become the dominant approach in this field [9]-[10]. While Inception-ResNet delivers impressive performance, models not tailored to specific scenarios often encounter issues like gradient vanishing, local minima, and overfitting. Therefore, enhancing Inception-ResNet through the incorporation of depthwise operations is imperative. By using depthwise operations, it enhances network efficiency and effectiveness by reducing parameter count and conserving computational resources by eliminating unnecessary parameters. [18].

The following are the significance of this project and potential contributions:

- Enhanced Breast Cancer Diagnosis Accessibility
- Improved Diagnosis Efficiency
- Reduced Misdiagnosis Rate
- Early detection and Prevention
- Conserved Medical Resources and Improved Allocation
- Increased Life Saving Rate
- Cost-Effective Healthcare Solutions
- Promotion of Public Health Awareness

1.4.2 Audience

The development of a specialized system for breast cancer diagnosis will bring about significant benefits to various stakeholders.

Medical Professionals: Radiologists and oncologists will benefit from the enhanced accuracy and efficiency of breast cancer diagnosis. The CNN can aid in early detection, reducing the chances of misdiagnosis and allowing for more timely

interventions.

Hospitals and Clinics: Healthcare institutions will experience improved workflow and reduced diagnostic errors, which can lead to better patient care and outcomes. It can also streamline the diagnostic process, potentially reducing the burden on healthcare resources.

Breast Cancer Patients: Patients will benefit from faster and more accurate diagnosis, resulting in quicker treatment initiation and improved chances of survival. Additionally, reduced false positives and negatives can alleviate the emotional stress associated with diagnostic uncertainty.

Medical Researchers: Researchers can access a valuable tool for analyzing a vast amount of medical imaging data, facilitating advancements in breast cancer research and treatment methods.

In summary, the proposed depthwise-Inception-ResNet-attention model promises benefits for medical professionals, healthcare institutions, breast cancer patients, and the broader research community by enhancing the accuracy, efficiency, and overall quality of breast cancer diagnosis and care.

Chapter 2 Background Review

Various researchers have proposed different networks for the enhancement of the classification of breast cancer. This section will present works that had been done for breast cancer classification by numerous researchers.

Hirra et al., [1] proposed Pa-DBN-BC, a patch-based deep learning method, achieving 86% accuracy in diagnosing cancer from histopathology images. Sahu et al.,[9] introduced a model trained on mini-DDSM, yielding 99.17% and 97.75% accuracy for abnormalities and malignancy. Liang and Meng [19] achieved high accuracy in binary and eight-class classification with BreakHis datasets. Alkhaldi and Salari utilized ensemble optimization, attaining 92.874% accuracy in Invasive Ductal Carcinoma classification [20].

Xu et al., [21] introduced an attention mechanism network with 98% accuracy, albeit limited by the smaller BreakHis dataset. Wu et al. [22] trained on 224,426 mammography images, reaching an AUC of 0.895. Chougrad et al. [23] employed transfer learning, achieving 98.94% accuracy post-merging datasets. Yu et al. [24] used SCDA data augmentation with ResNet-50, obtaining 95.74% accuracy, 98.55% specificity, and 92.83% sensitivity. Arya and Saha [25] developed a stacked-based ensemble model with 90.2% accuracy for breast cancer prognosis. Whitney et al. [10] highlighted the efficacy of CNN transfer learning in diverse imaging modalities for accurate breast cancer diagnosis.

Chattopadhyay et al., [26] developed the MTRRE-Net, a deep learning model, for breast cancer detection from histopathological images, demonstrating superior accuracy with up to 97.81% on various magnification levels of the BreakHis dataset, showcasing its effectiveness in medical diagnostics.

Addo et al., [27] introduced BCHI-CovNet, a novel lightweight AI model for classifying histopathological breast cancer images, achieving remarkable accuracies: 99.15% at 40X magnification, 99.08% at 100X, 99.22% at 200X, and 98.87% at 400X on the BreaKHis dataset, and 99.38% on the BACH dataset. A summary of the different researchers and their findings and possible results can be found in Table 1.

Author	Datasets	Methods	Results
Hirra et al. [1]	Histopathology images	Patch-based deep learning & Deep belief Network	Acc = 86%
Sahu et al. [9]	Mini-DDSM	AlexNet +ResNet +MobileNeetV2	Abnormalities: Acc = 99.17% Malignancy: Acc = 97.75%
Liang and Meng [19]	BreakHis	Convolutional Block Attention Module and Convolutional Multi-Layer Perceptron	Acc = 95.5%
Alkhaldi and Salari [20]	Invasive-Ductal -Carcinoma (IDC)	Multi-ResNet CNN	Acc = 92.874%
Xu et al. [21]	BreakHis	DeNet	Acc = 98%
Wu et al. [22]	224,426 mammography	Ensemble of Four ResNets	AUC = 89.5%
Chougrad et al. [23]	INbreast, DDSM, BCDR	VGG16, ResNet50, InceptionV3	DDSM: Acc = 97% AUC = 98% INbreast: Acc = 95.5% AUC = 97% BCDR: Acc = 96.67% AUC = 96% Independent database (MIAS): Acc = 98.23% AUC = 99%
Yu et al. [24]	INbreast, mini-DDSM	SCDA augmentation & ResNet-50	Acc = 95.74% Spec = 98.55 Sens = 92.83%
Arya and Saha [25]	1,980 patients' breast cancer data	stacked ensemble model	Acc = 90.2% AUC = 0.93
Chattopadhyay et al., [26]	BreakHis	MTRRE-Net	All in Acc 40X: 97.12%

			100X: 95.2% 200X: 96.8% 400X: 97.81%
Addo et al., [27]	BreakHis	BCHI-ConvNet	All in Acc 40X: 99.21 % 100X: 99.10 % 200X: 99.36 % 400X: 98.93 %

Table 1: Summary of Related Works

Chapter 3 Methodology

3.1 Approach

The proposed CNN model comprises two individual models with two mechanisms.

The basic idea is to combine Inception-V4 Model, Residual Network, and integrate attention mechanism and depthwise convolution which are respectively used to concentrate on relevant features and to reduce the computation resources.

3.1.1 Model Construction

In this phase, the model will be separated into their single model, dual connection model and down to the formation of the proposed model called DIRA-Net in the subsequent subsection.

3.1.1.1 Inception Network Version 4

Inception V4, as shown in Figure 7 to Figure 9, introduced by Google researchers in 2016, is a deep learning architecture renowned for its advanced techniques, including inception modules that efficiently learn local and global features using filters of varying sizes. It excels in image recognition and offers scalability [28].

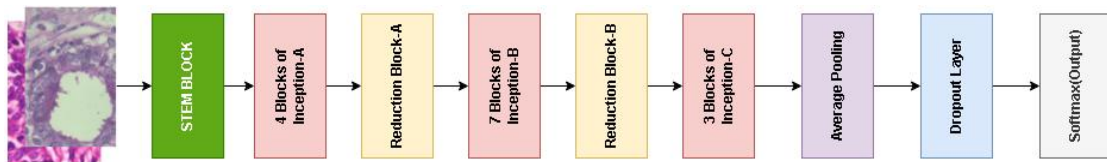


Figure 7: Inception V4 Architecture

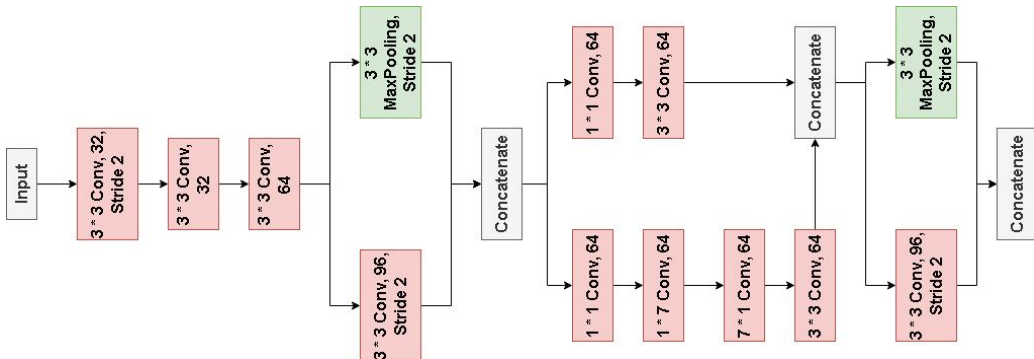
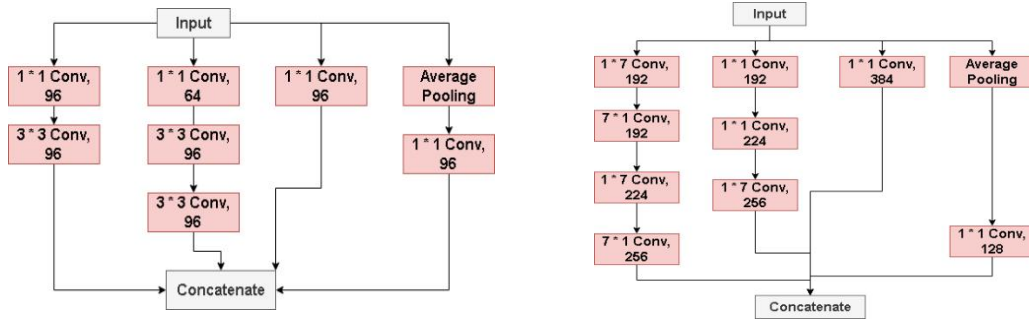
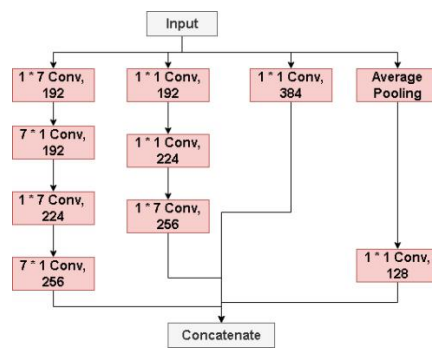


Figure 8: InceptionV4 STEM Block

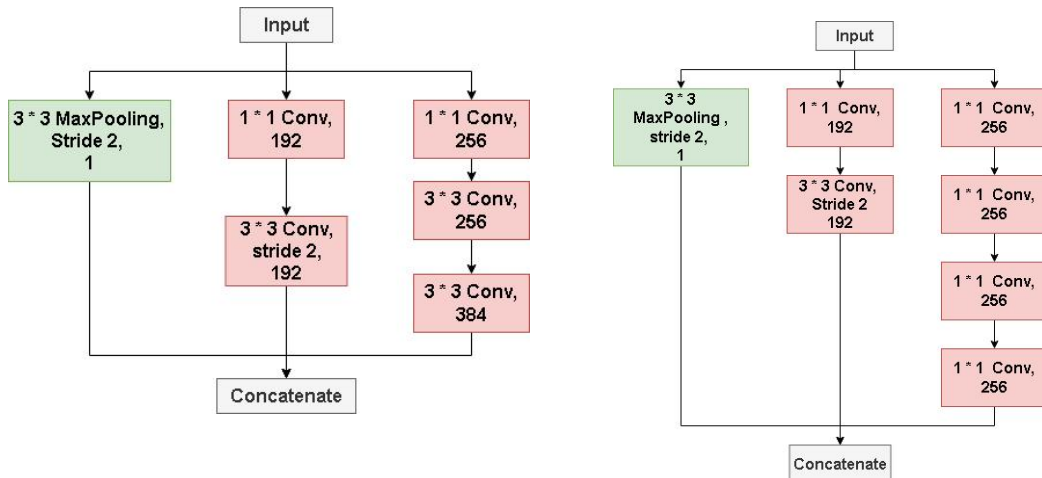


a) Inception Block A

b) Inception Block B



c) Inception Block C



d) Reduction Block A

e) Reduction Block B

Figure 9: a) to e) demonstrate the basic structure of each block within the original Inception V4 which includes three traditional inception block and two parameters reduction block.

3.1.1.2 Residual Network

ResNet blocks, as illustrated in Figure 10, were introduced to incorporate residual connections, effectively mitigating gradient-related challenges in deep networks and leading to enhanced training efficiency [29].

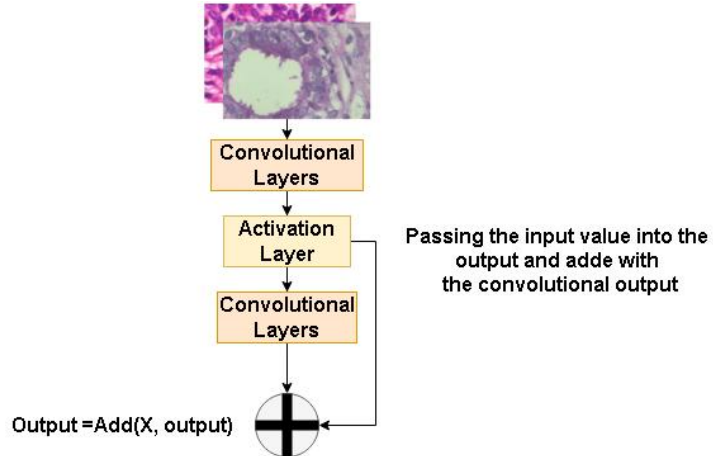


Figure 10: Basic ResNet Block

3.1.1.3 Depthwise Convolution Model

Depthwise Convolution as provided in Figure 11 is a convolutional approach that separates convolution into channels to reduce computational load and parameters while preserving input spatial resolution and efficiency [30].

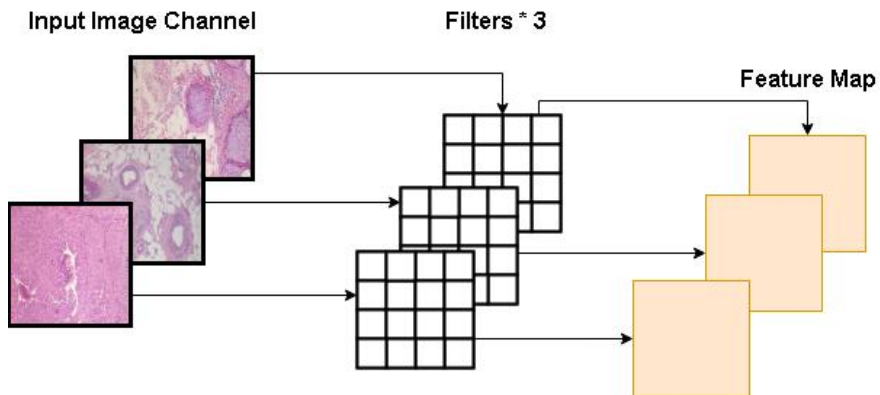


Figure 11: Depthwise Convolution

3.1.1.4 Attention Mechanism

Networks with attention mechanisms, displayed in Figure 12 focus on specific areas for more relevant task-related features [31]. Attention combines a reference with keys to calculate scores, which are then used to determine importance, allowing concentration on specific information. The equations are provided from Equation (5) to

Equation (7).

$$\text{Attention Score } (Q, K) = Q * K^T \quad \text{Equation (5)}$$

$$\text{Attention Weights } (Q, K) = \text{softmax}(\text{Attention Score } (Q, K)) \quad \text{Equation (6)}$$

$$\text{Attention Values } (Q, K, V) = \text{Attention Weights}(Q, K) * V \quad \text{Equation (7)}$$

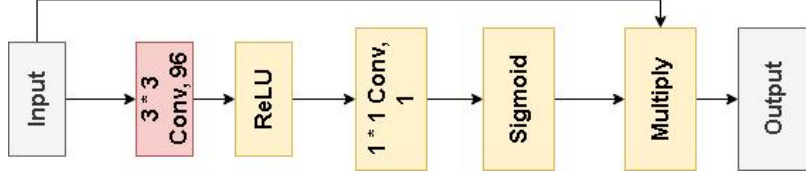


Figure 12: Attention Block

3.1.1.5 Inception-ResNet Model

Figure 13 to Figure 15 illustrate the fusion of Inception with ResNet Blocks, creating the prototype Inception-ResNet Blocks structure of this project. This hybrid design incorporates the multi-path feature extraction of Inception with the gradient-enhancing properties of ResNet. By combining these elements, Inception-ResNet Blocks enable efficient learning of intricate features, leading to more accurate and effective deep learning models [29]. The diagram showcases the amalgamation of these techniques, highlighting their collaborative strength in enhancing the network's capabilities.

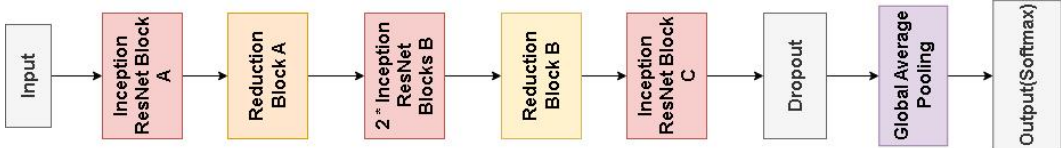


Figure 13: Inception-ResNet-Prototype

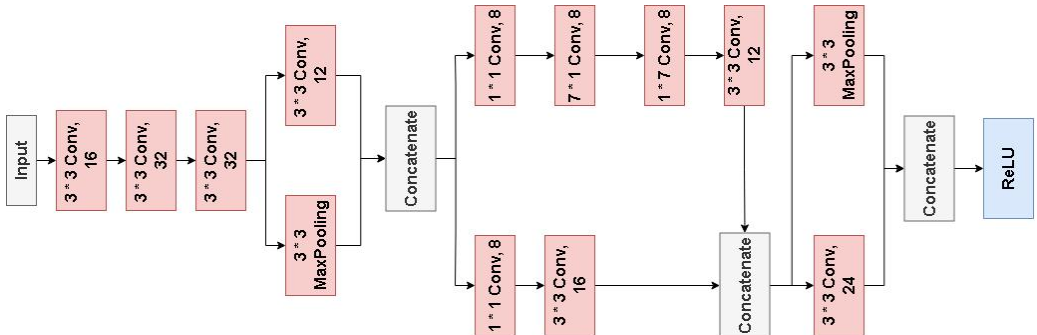
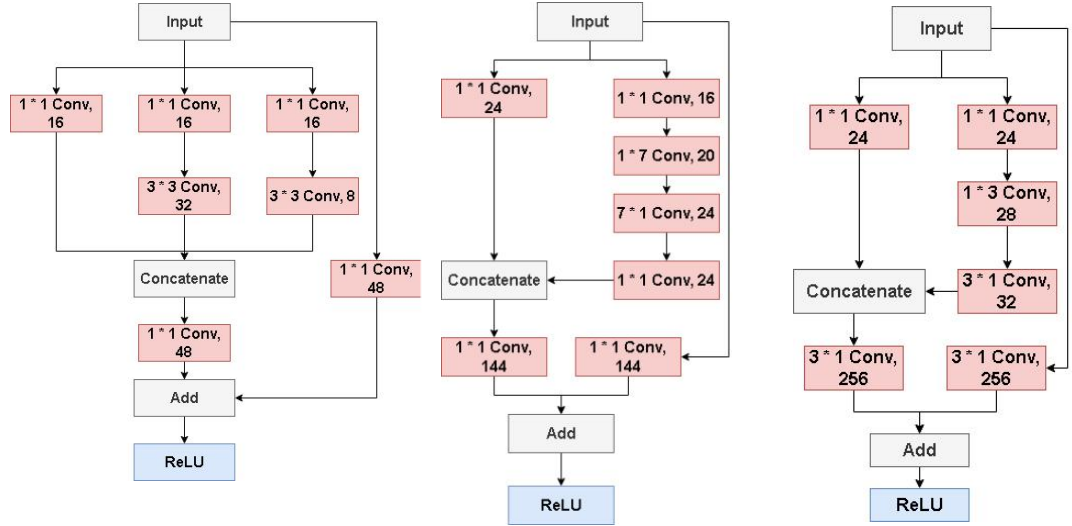


Figure 14: STEM Block of Inception-ResNet Prototype Model

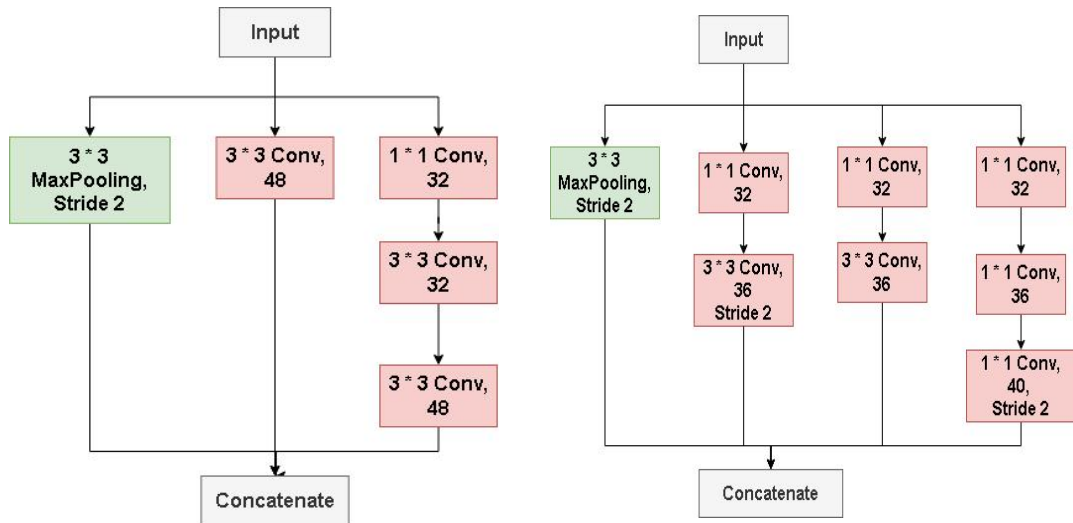


a) Inception-ResNet-Block-A

b) Inception-ResNet-

c) Inception-ResNet-

Block-C



d) Inception-ResNet-Reduction-Block-A

e) Inception-ResNet-Reduction-Block-B

Figure 15: a) to e) showcases the detail structure of Inception-ResNet model

3.1.1.6 Depthwise-Inception-ResNet Model

In order to increase the complexity and while keeping the parameters within a reasonable range, depthwise convolution operation is added to the IR-Block A. And other blocks remain the same. Figure 16 demonstrates the integration of Depthwise mechanism within the IR-Block A.

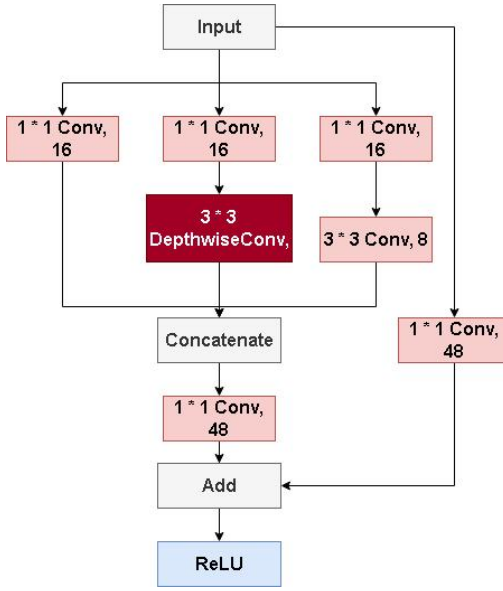


Figure 16: Depthwise-Inception-ResNet Model

3.1.1.7 Depthwise-Inception-ResNet-Attention Model

At last, the model is improved through integrating attention mechanism into the STEM block which is placed in Figure 17 so as to create valuable feature map. Other blocks remain the same as above.

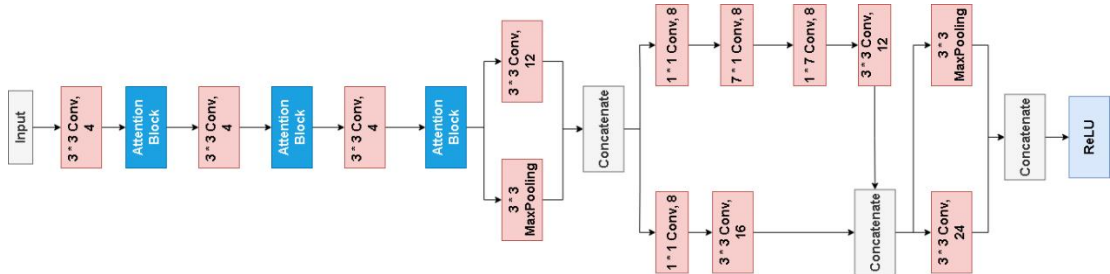


Figure 17: Depthwise-Inception-ResNet STEM block with attention mechanism

3.1.1.8 The Proposed Model

Figure 18 depicts the proposed model, DIRA-Net, which integrates the Attention STEM block, DIR-Block A, IR-Block B, IR-Block C and two IR-Reduction blocks. It combines Depthwise convolution, Inception, Residual blocks, and an Attention mechanism within the STEM to provide a robust solution for complex tasks like breast cancer image classification. It addresses the issue of gradient vanishing in deep networks by leveraging residual connections from IR-blocks. The proposed model achieved parameter efficiency by separating channel from spatial dimensions,

reducing the number of parameters without sacrificing the performance. The integration of Attention STEM block enhanced with L2 regularization can capture nuanced features and prevent overfitting in training. Furthermore, He_normal initialization is applied at each layer to ensure effective weight setting from the outset. This architectural modification promotes precision and complexity management while maintaining a lean parameter profile, increase computational efficiency. And thus, this model is particularly suitable for deployment on devices with limited computational capabilities in medical field.

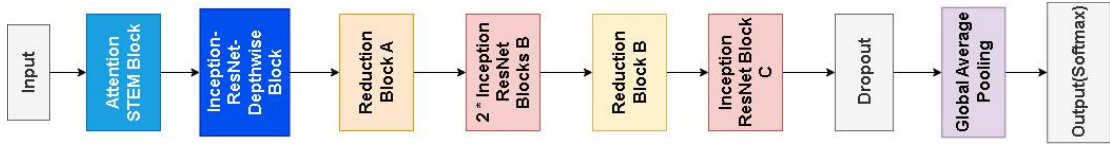


Figure 18: The proposed model DIRA-Net

3.2 Dataset

Following will be providing crucial information about the dataset this project used.

3.2.1 Dataset Introduction

During the training process, BreakHis will be the main dataset used for model training. The BreakHis dataset provides 9,109 histopathological images from 82 patients, categorized into 2,480 benign and 5,429 malignant samples at magnifications of 40X to 400X. Each RGB image has a resolution of 700 * 460 pixels. This dataset, created with the P&D Laboratory in Parana, Brazil, is instrumental for benchmarking in medical image analysis. It differentiates between non-invasive benign tumors and invasive malignant tumors capable of metastasis. Breast tumors are subtyped into adenosis, fibroadenoma, phyllodes tumor, and tubular adenoma for benign, and ductal carcinoma, lobular carcinoma, mucinous carcinoma, and papillary carcinoma for malignant, enabling detailed research studies. The nomenclature of each image provides insights into the biopsy type, tumor classification, patient ID, and magnification used. Figure 19 displays examples of BreakHis images.

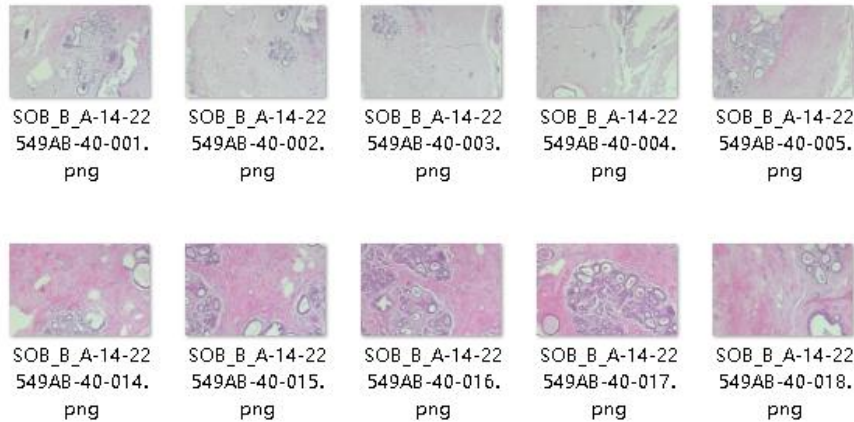


Figure 19: Examples of BreakHis Images

3.2.2 Data Separation

The BreakHis file has four symptoms in each benign and malignant. And each symptom contains four different magnifications. In the case that binary classification is the main goal of the project, the data are separated based on the magnifications of images. Then, inside each magnification, there are “train” folder and “test” folder which all contain benign and malignant. The above maneuver was completed through Python codes which had imported PIL (Pillow library) specialized for file management. After copying the file into corresponding directories, data are then split using a random file selecting Python code to randomly move a proportion of images into test folders so as to reach the ratio of 85% : 15% between train folder and test folder. Rest of the separation of validation and training data will be done within the model, which will dynamically select 15% of the total images from the training set for validation during each training session, ultimately achieving a distribution of 70% for training, 15% for validation, and 15% for testing. The structure of the data separation is provided in Figure 20.

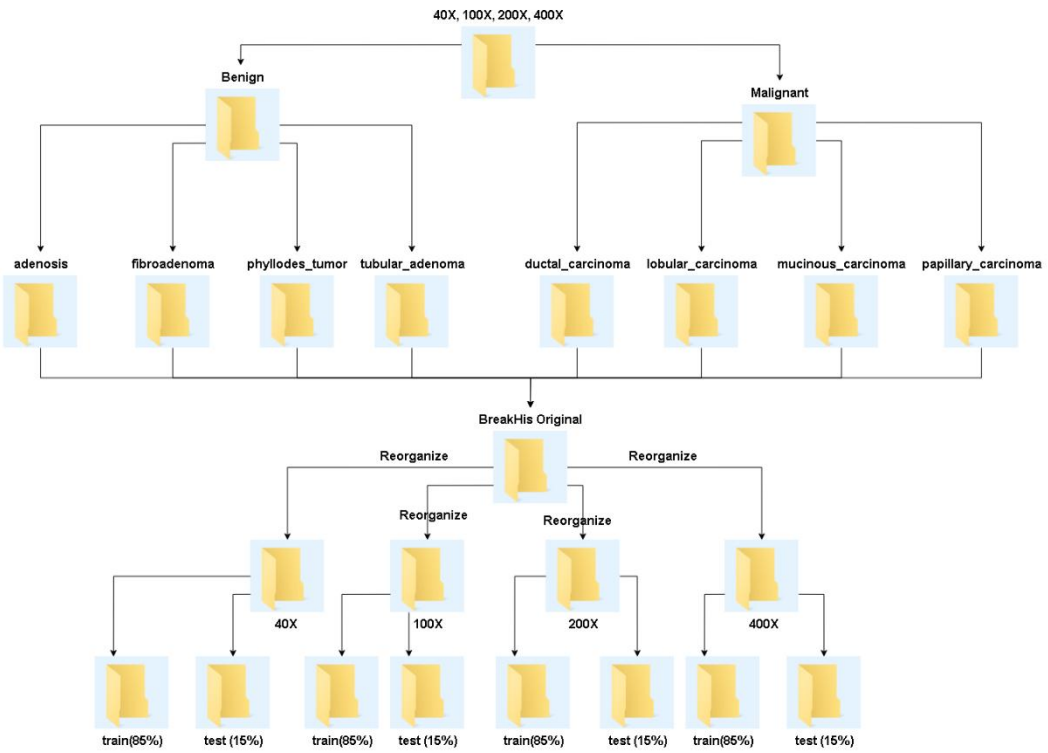


Figure 20: Dataset Structure after Separation

3.2.3 Data Balance

Firstly, based on the Figure 21 provided below, it is noticeable that within each magnification folder, the benign images are far less than malignant images, which makes the data unbalanced. Therefore, this project had applied oversampling to balance the dataset, which is shown in Figure 22.

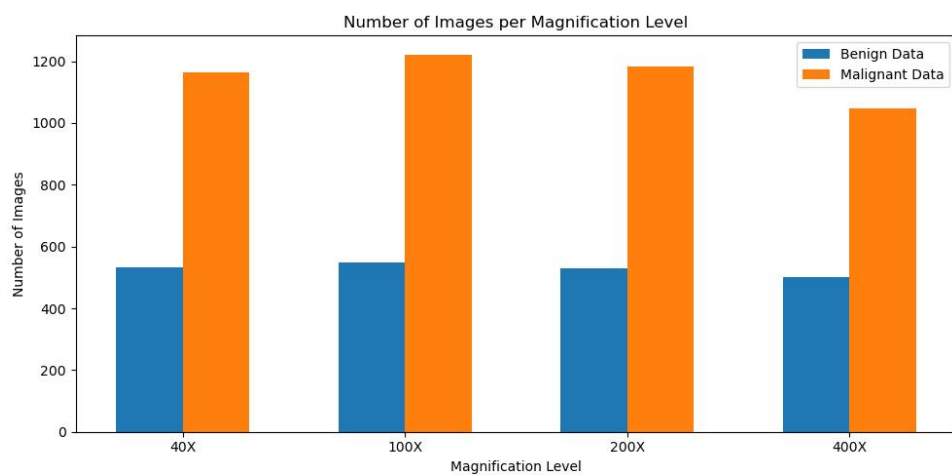


Figure 21: Number of images within Benign and Malignant Before Balancing

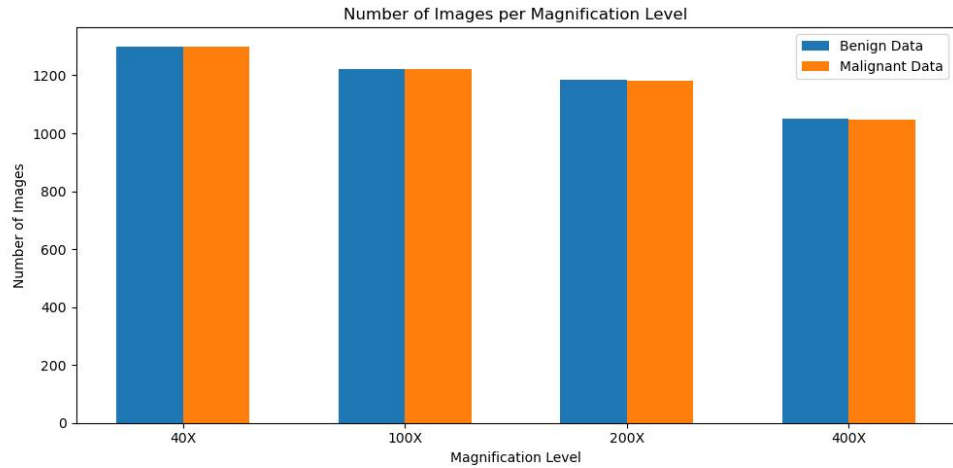


Figure 22: Images Number After Balancing

3.2.4 Data Resize

As the introduction mentioned, the image resolution is $700 * 460$ pixels, which does not fit in the proposed model input. And therefore, this project had resize the images of all magnifications into $224 * 224$.

3.2.5 Data Color Channel Modification

This project had modified the images utilizing Contrast Limited Adaptive Histogram Equalization (CLAHE) which are then compared with the original image training results in order to select the better one. CLAHE operates by adaptively dividing the image into several small blocks, then performing histogram equalization on each of these blocks within certain contrast limits [32]. This approach improves the histogram distribution of the image, which is essential for enhancing detail and image quality.

Images are displayed in the following Figure 23.

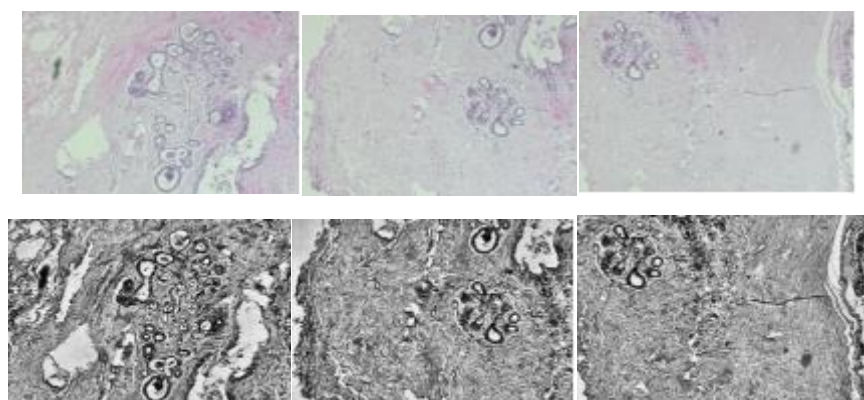


Figure 23: Images Transformation

3.2.6 Data Augmentation

The BreakHis dataset is augmented with rotations (20 degrees), shifts (20% width and height), shear (20%), zoom (20%), and horizontal flips, alongside rescaling the pixel values by 1/255. Figure 24 displays the augmentation of the image.

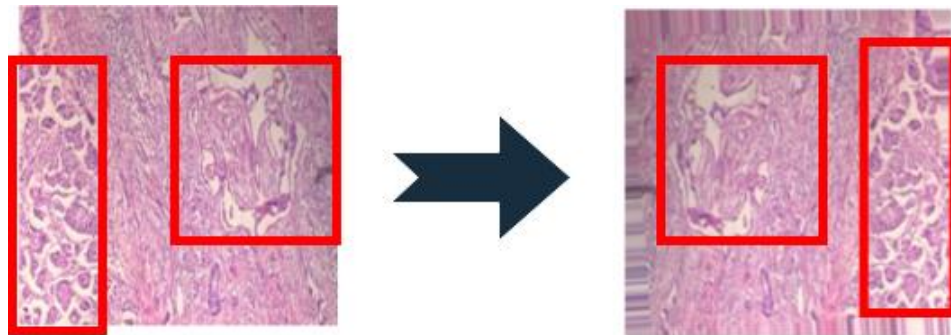


Figure 24: Augmented image example

3.2.7 Data Preprocessing Summary

Table 2 displays the numbers of images after upsampling and are then used through the whole project. Table 3 shows the augmentation.

Magnification	Train		Test		Total
	Benign	Malignant	Benign	Malignant	
40X	1300	1300	93	205	2898
100X	1200	1222	96	215	2733
200X	1180	1182	93	208	2663
400X	1050	1048	88	184	2370

Table 2: Upsampling detail for each magnification

Magnification	RR	WS	HS	SR	ZR	HF	FM
40X	0.2	0.2	0.2	0.2	0.2	True	Nearest
100X	0.2	0.2	0.2	0.2	0.1	True	Nearest
200X	0.4	0.3	0.2	0.3	0.1	True	Nearest
400X	0.4	0.1	0.1	0.1	None	True	Nearest

Table 3: Different Augmentation of Different Magnification

3.3 Technology

The technology used in this project is displayed in Table 4

Software	Framework	Tensorflow 2.9.0 CuDNN 8.9 Cuda 11.2
	Language	Python 2.9.0
	Libraries and Application	Numpy 1.25.3 Keras 2.9.0 Matplotlib 3.7 TensorFlow-Addons 2.10.0
	Cloud Repository	Github Repository
	Central Processing Unit(CPU)	Intel(R) Core(TM) i7-8750H CPU @ 2.2GHz(12 CPUs), ~2.2GHz
	Graphic Processing Unit(GPU)	NVIDIA GeForce GTX2060

Table 4: Summary of Relevant Technology involved in this project

3.4 Data Testing and Evaluation Plan

3.4.1 Data Testing

By checking the BreakHis datasets downloaded from Kaggle, it is estimated that some techniques of data pre-processing will be implemented which will be displayed below.

- 1 This project will re-divide the original BreakHis datasets for binary classification. Considering the fact that there are four groups of magnifications of the histogram, this project will create four magnifications which contains two categories of breast cancer level from the original datasets.
- 2 The project will check the image size inside each magnification category and ensure the size of images are consistent, otherwise, resize techniques will be applied.
- 3 The project must separate the data into specific ratio for the purpose of

training, validation and testing.

- 4 This project must check the number of each set, aimed at balancing the two categories. It will affect the model learning and diagnosis accuracy otherwise.
- 5 This project will apply methods of data pre-processing on the datasets and test on model training in case there are any factors such as color or contrast that affects training results.

3.4.2 Model Performance Evaluation Criteria

This project will evaluate the performance of the model through following standards.

Accuracy: Accuracy is a quite intuitive metric and a criteria for evaluating model performances, which displays the overall correctness of a classification model. It calculates the ratio of the correctly predictions among the total predictions. The Equation (8) is displayed below, where T, P, N, F represents, true, positive, negative and false. TP, TN, FP, and FN represent the counts of correctly identified positive cases, correctly identified negative cases, incorrectly identified positive cases, and incorrectly identified negative cases, respectively, in a classification model.

$$Accuracy = \frac{TP + TN}{TP + TN + FP + FN} \quad \text{Equation (8)}$$

Loss: This criteria measures the gap between results of prediction labels and actual labels. Below shows Equation (9) for classification.

$$Loss = \sum_{c=1}^M y_{ic} \log(p_{ic}) \quad \text{Equation (9)}$$

Precision: This is the criteria that shows the proportion of images that are positively classified as positive. Equation (10) is shown below.

$$Micro Precision = \frac{\sum_{i=1}^n TP_i}{\sum_{i=1}^n TP_i + \sum_{i=1}^n FP_i} \quad \text{Equation (10)}$$

Recall: This is the criteria that displays the proportion positively identified as positive samples among the actual positive samples. Equation (11) depicts recall calculation.

$$Micro Recall = \frac{\sum_{i=1}^n TP_i}{\sum_{i=1}^n TP_i + \sum_{i=1}^n FN_i} \quad \text{Equation (11)}$$

F1-Score: F1-Score measures the performance of model by calculating the harmonic mean of Precision and Recall. Equation (12) illustrates F1-Score calculation.

$$Micro F1 - Score = \frac{2 * Micro Precision * Micro Recall}{Micro Precision + Micro Recall} \quad \text{Equation (12)}$$

Confusion Matrix: It displays the accurate number of the True Positive, True Negative, False Positive and False Negative.

ROC: Receiver Operating Characteristic (ROC), which displays the trade-off relationships between the True Positive Rate(also known as sensitivity or recall) and the False Positive Rate of a model at different thresholds.

AUC: Area Under the ROC curve, which demonstrates the overall ability to distinguish between positive and negative samples. In the classification circumstance, AUC acts as metric to evaluate the performance of model for both classes. Generally speaking, a model is considered well performed when the curve rises towards the upper-left corner of the graph, and therefore, leaving more space to AUC. In a nut shell, the closer AUC gets to 1, the better the model is.

In summary, in order to evaluate the model performance on the binary classification of the level of breast cancer, this project will conduct a comprehensive evaluation, involving Accuracy, Loss, Precision, Recall, Precision-Recall Graph, F1-Score, Confusion Matrix, ROC graph, and AUC.

Chapter 4 Experiment and Results

4.1 Experiment Phases

- 1 Testing each single model such as InceptionNet, ResNet, DepthwiseNet on the pre-processed dataset with 40X, 100X, 200X and 400X magnification. And therefore deciding which magnification is the best to train on.
- 2 Select the best magnification and train the model of IR-Net on the selected magnification of the dataset.
- 3 Build and train the DIR-Net on the selected magnification.
- 4 Build and train the DIRA-Net on the selected magnification.
- 5 Fine tune the model to achieve a better result and compare with the existed pre-trained model.
- 6 Existing pre-trained model comparison and results comparison with previous Work.

4.2 Inception-Net Training on Four Magnification

The first two individual models provide not only the initial judgement of the performance on the BreakHis dataset, but also insights of which magnification works better for model training.

The pure Inception-Net is trained with original (700 * 460) and resize (244 * 244) version images which help deciding which scale of images should remained for further training. Model structure is provided in Figure 25.

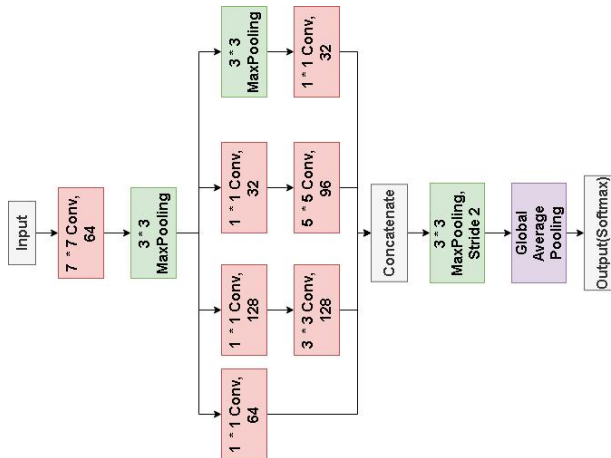
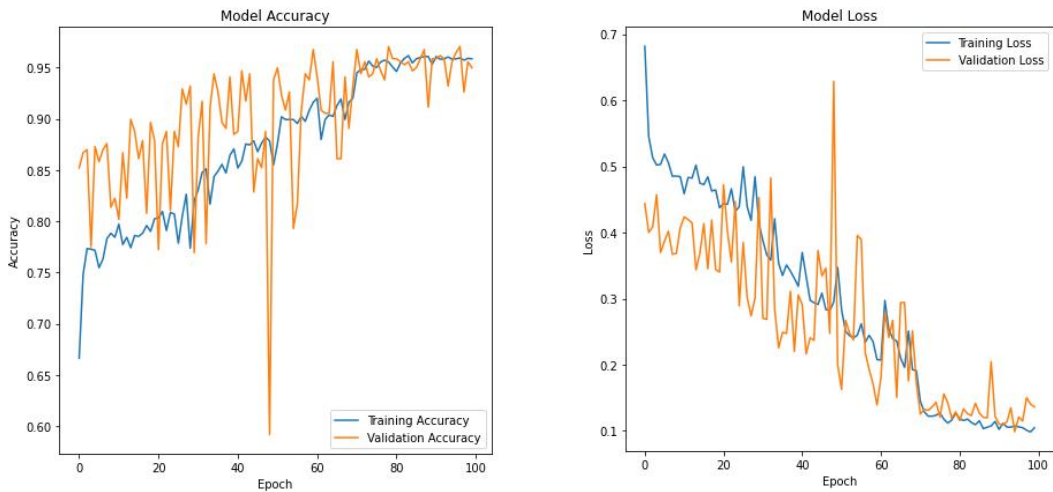


Figure 25: Initial Inception Model for experiment

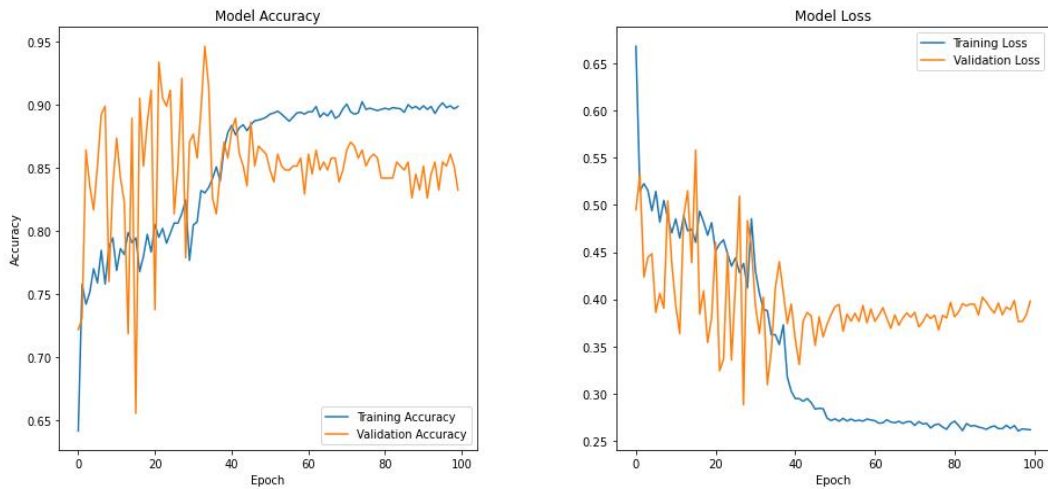
Figure 26 to Figure 29 show the results of Inception-Net training on raw images.



a) Train Acc = 0.9584, Val Acc = 0.9497

b) Train Loss = 0.1047, Val Loss = 0.1362

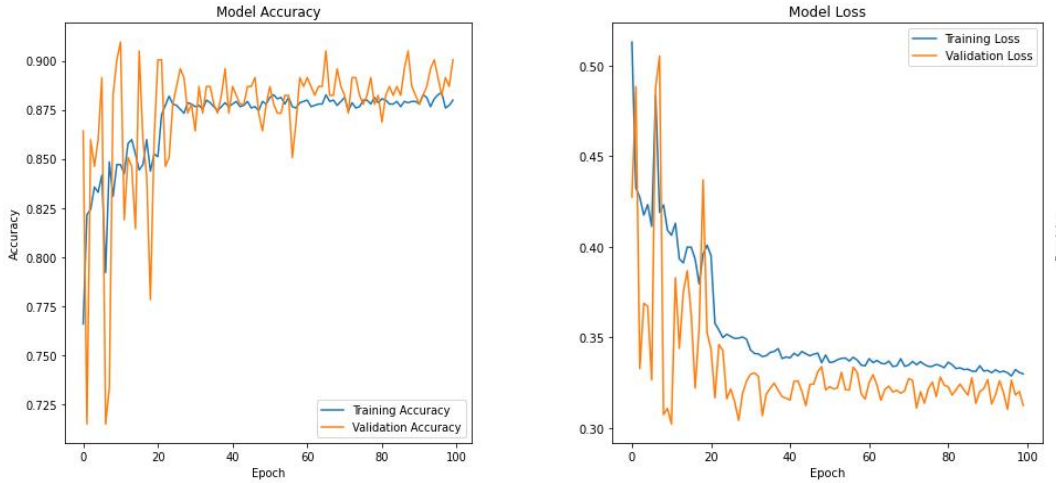
Figure 26: a) and b) present InceptionNet Accuracy and Loss of Train and Validation sets on 40X Raw Images



a) Train Acc = 0.8985, Val Acc = 0.8323

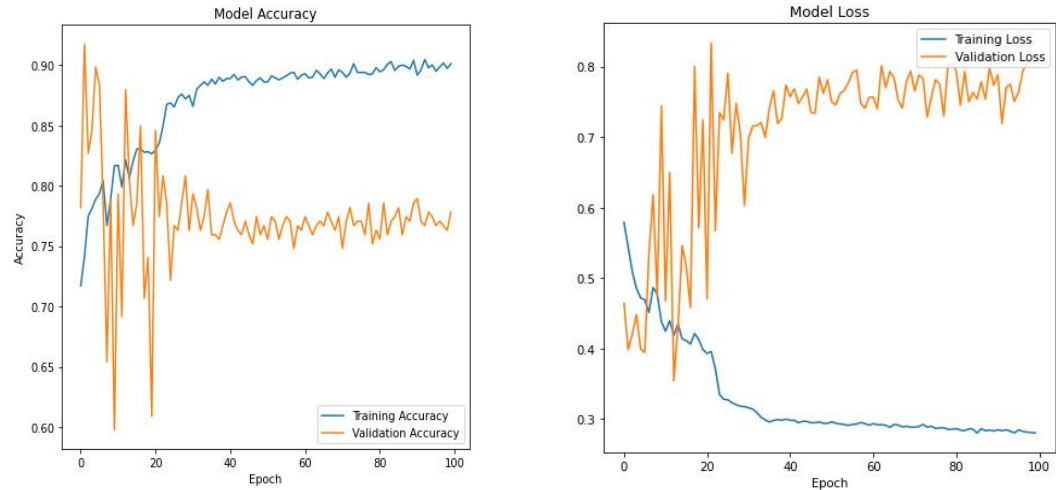
b) Train Loss = 0.2617, Val Loss = 0.3980

Figure 27: a) and b) display the InceptionNet Train and Validation Accuracy and Loss on 100X Raw Images



a) Train Acc = 0.8799, Val Acc = 0.9005 b) Train Loss = 0.3298, Val Loss = 0.3123

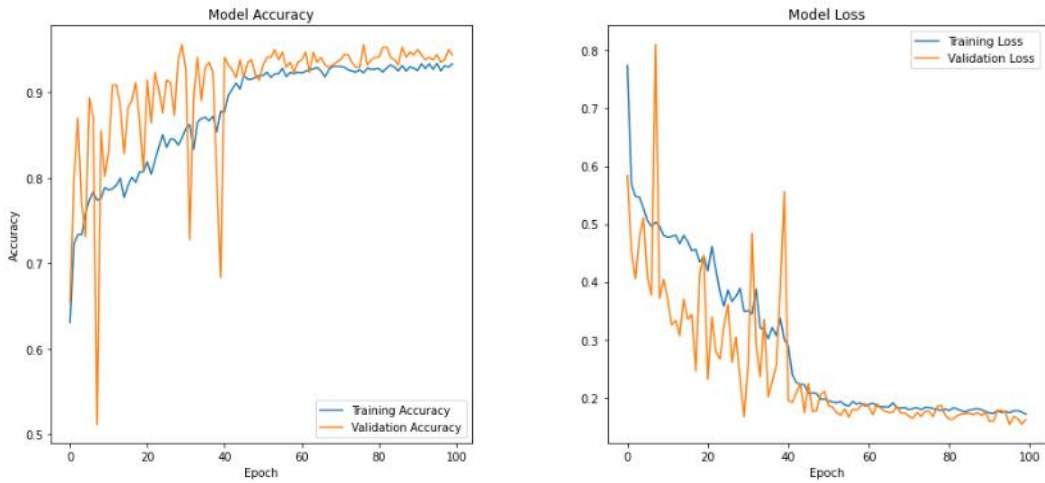
Figure 28: a) and b) illustrate InceptionNet Train, Validation Accuracy and Loss on
200X Raw Images



a) Train Acc = 0.9012, Val Acc = 0.7782 b) Train Loss = 0.2804, Val Loss = 0.8079

Figure 29: a) and b) demonstrate InceptionNet Train, Validation Accuracy and Loss on
400X Raw Images

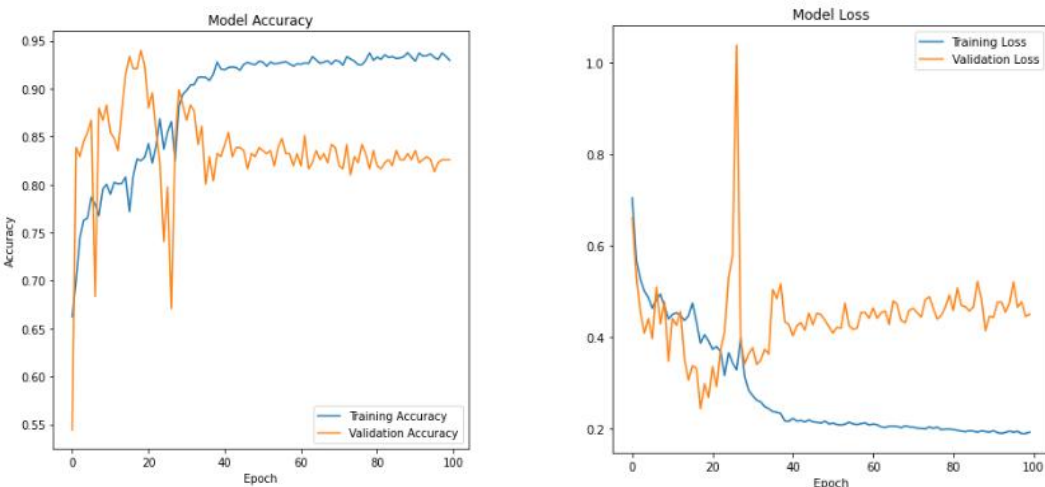
Based on Figures 26 to 29, it is evident that without resizing the images, the model's performance during training varies among four magnification factors: 40X, 100X, 200X, and 400X. Notably, the model exhibits the best fitting performance when trained on images with a 40X magnification factor among these four options.



a) Train Acc = 0.9332, Val Acc = 0.9438 b) Train Loss = 0.1709, Val Loss = 0.1617

Figure 30: a) and b) display InceptionNet Train, Validation Accuracy and Loss on 40X

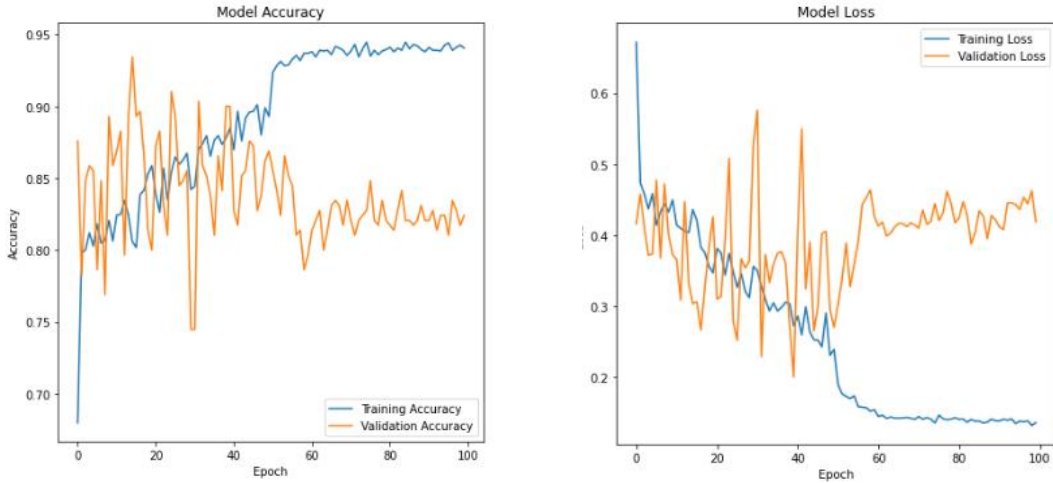
Resize Images



a) Train Acc = 0.9295, Val Acc = 0.8259 b) Train Loss = 0.1918, Val Loss = 0.4495

Figure 31: a) and b) display InceptionNet Train, Validation Accuracy and Loss on 100X

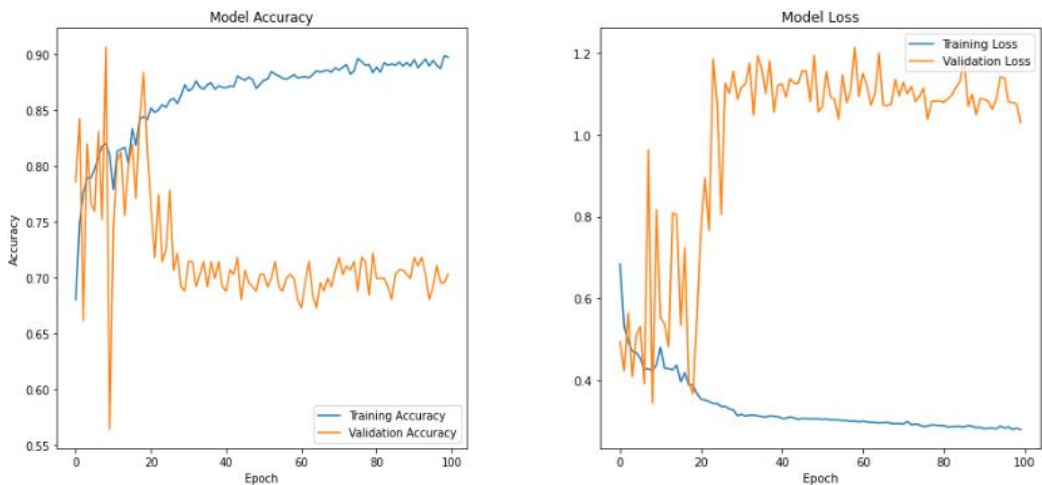
Resize Images



a) Train Acc = 0.9406, Val Acc = 0.8241 b) Train Loss = 0.1361, Val Loss = 0.4191

Figure 32: a) and b) present InceptionNet Train, Validation Accuracy and Loss on 200X

Resize Images



a) Train Acc = 0.8973, Val Acc = 0.7030 b) Train Loss = 0.2782, Val Loss = 1.0301

Figure 33: a) and b) demonstrate InceptionNet Train, Validation Accuracy and Loss on

400X Resize Images

In Figures 30 to Figure 33, after resizing the images to a size of 224 x 224 pixels to match the model input settings for this project, it is observed that, under the same four scenarios, the training performance of images with a 40X magnification factor continues to outperform the other three magnification factors.

However, considering Figure 34 and Figure 35, it becomes evident that most of the resized results surpass those without resizing. Furthermore, within this context, the training performance of images with a 40X magnification factor stands out as the most

favorable. This phenomenon may be attributed to the fact that, at this magnification level, more details are captured, resulting in a richer set of features. The upcoming experiment will further validate the suitability of magnification factors on resized images.

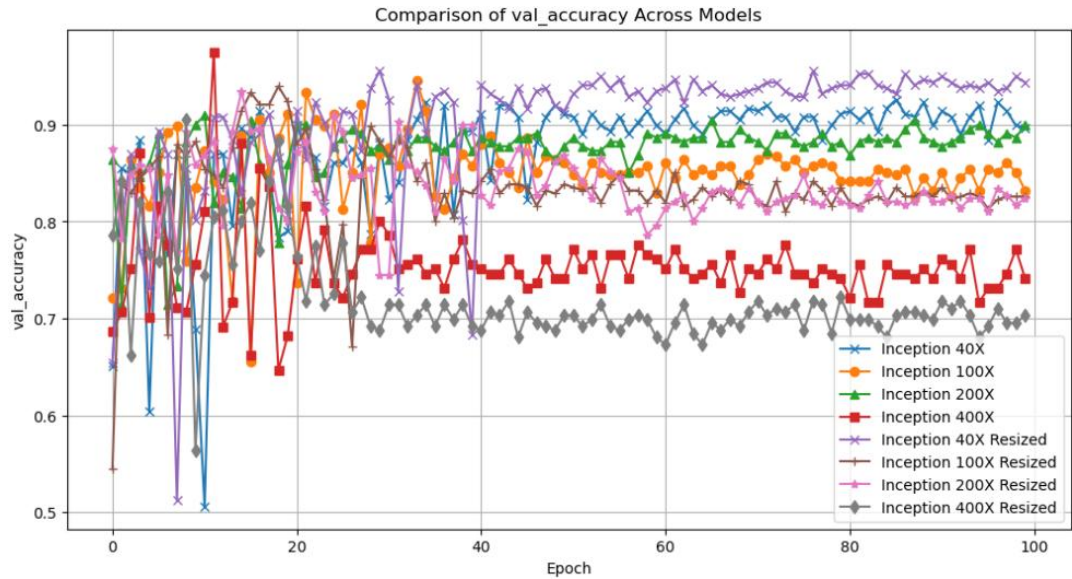


Figure 34: Comprehensive Comparison of Validation Accuracy Among Raw and Resized Images of Four Magnifications

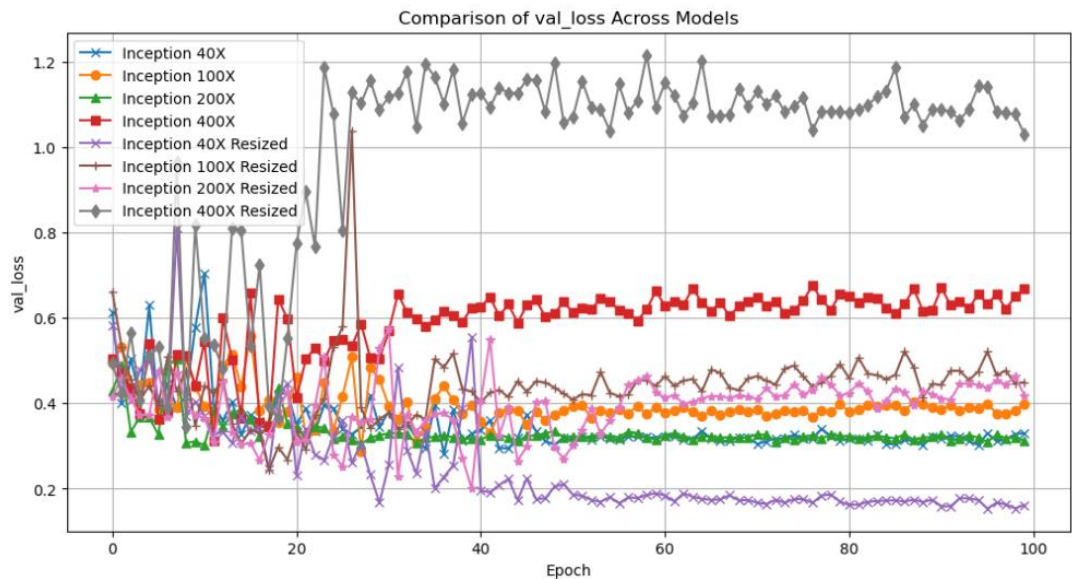


Figure 35: Comprehensive Comparison of Validation Loss Among Raw and Resized Images of Four Magnifications

4.3 ResNet Training on Four Magnification

Given that the final model will be complicated, with a large number of parameters, depth, and branching, gradient vanish is quite expected. Therefore, residual structure is examined on the dataset. The initial ResNet was trained on four magnifications with resized images based on the last part results. Model details and results are presented from Figure 36 to Figure 42.

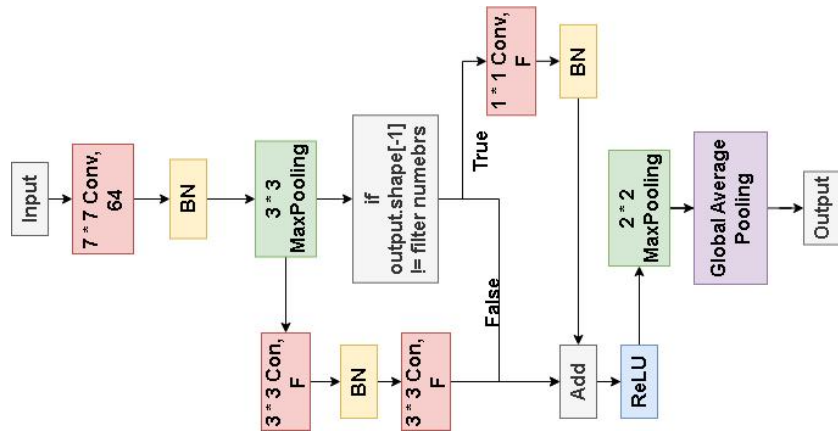
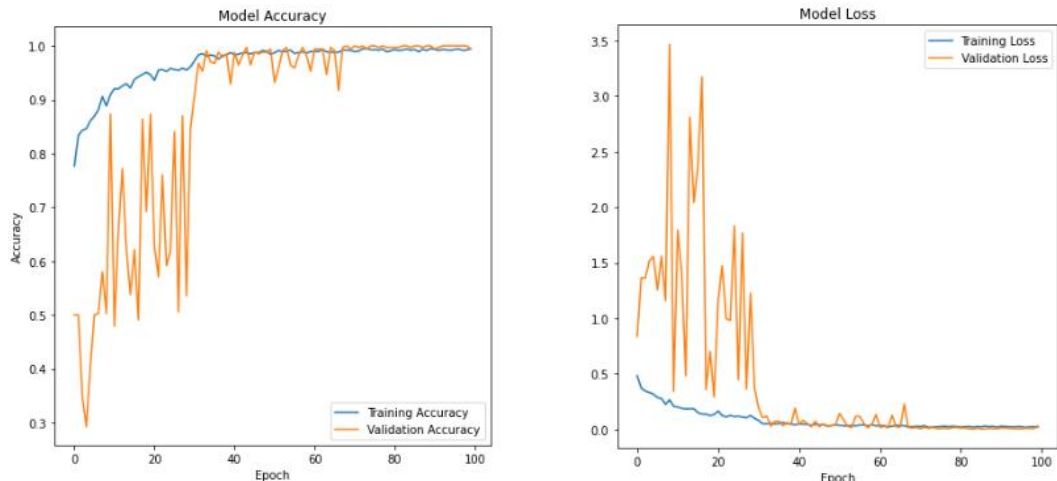
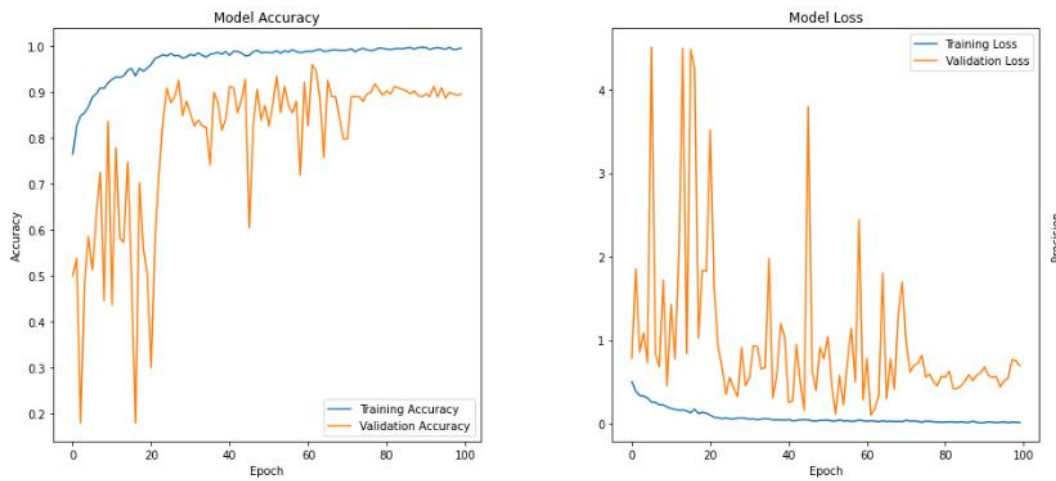


Figure 36: Initial ResNet for experiment



a) Train Acc = 0.9947, Val Acc = 0.9941 b) Train Loss = 0.0199, Val Loss = 0.0298

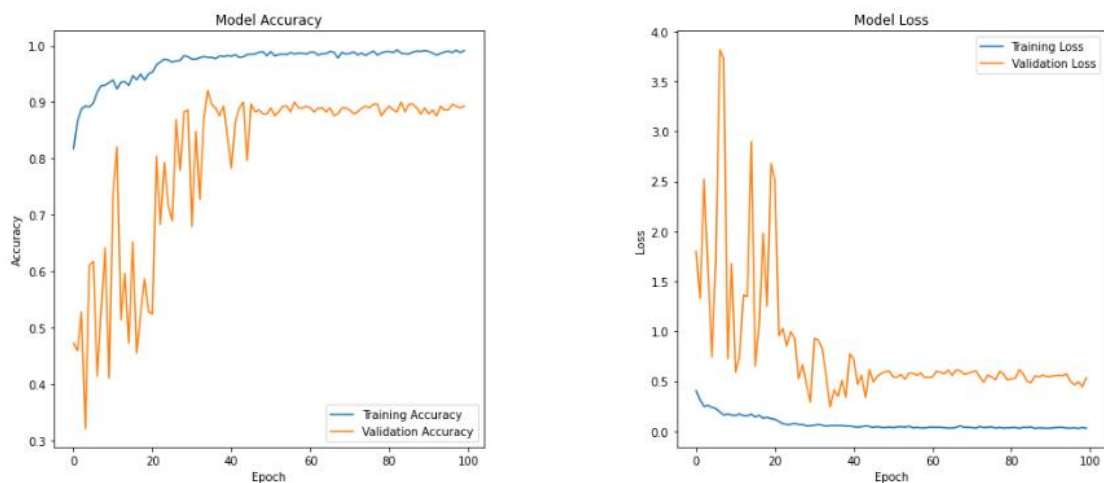
Figure 37: a) and b) illustrate ResNet Train, Validation Accuracy and Loss on 40X Resized Images



a) Train Acc = 0.9948, Val Acc = 0.8956 b) Train Loss = 0.0143, Val Loss = 0.6940

Figure 38: a) and b) display ResNet Train and Validation Accuracy and Loss on 100X

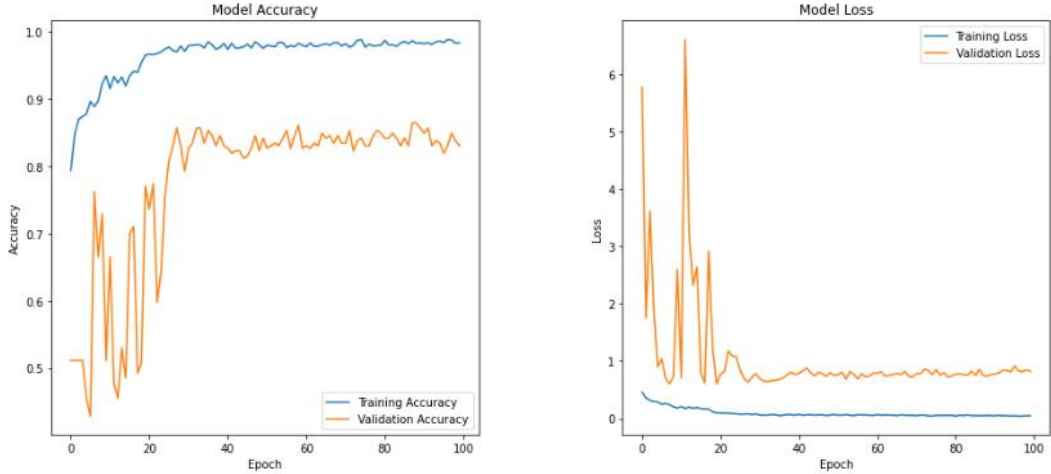
Resized Images



a) Train Acc = 0.9918, Val Acc = 0.8931 b) Train Loss = 0.0293, Val Loss = 0.5330

Figure 39: a) and b) display ResNet Train, Validation Accuracy and Loss on 200X Resized

Images



a) Train Acc = 0.9837, Val Acc = 0.8308 b) Train Loss = 0.0459, Val Loss = 0.8232

Figure 40: a) and b) display ResNet Train, Validation Accuracy and Loss on 400X
Resized Images

According to Figure 37 to Figure 40, the ResNet model's performance at various magnifications post-resizing reveals high training and validation accuracy rates at 40X, indicating successful feature capture. This is crucial for practical applications where the balance between resolution and recognizable features is delicate. However, at 100X, 200X, and 400X magnifications, there is a divergence between training and validation accuracy, suggesting overfitting. This could suggest the need for more complex models or refined training strategies to prevent the model from latching onto noise. Alternatively, sophisticated data preprocessing or augmentation techniques could help the model focus on relevant features.

Moreover, through the observation in Figure 41 and Figure 42, model's validation accuracy is best at 40X magnification, demonstrating minimal volatility. This balance captures enough detail for accurate classification without complexity. Future model development should focus on 40X magnification, aligning with the model's strengths and aiming for efficient diagnostic accuracy. This approach could simplify learning features, enhance predictive performance, and potentially increase clinical value.

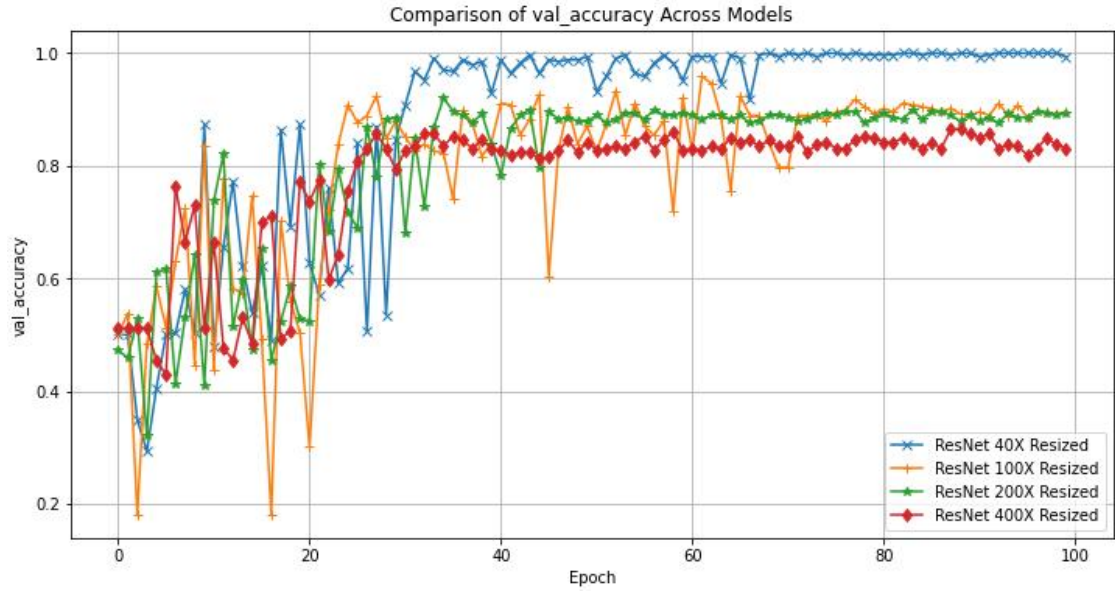


Figure 41: ResNet Validation Accuracy Comparison

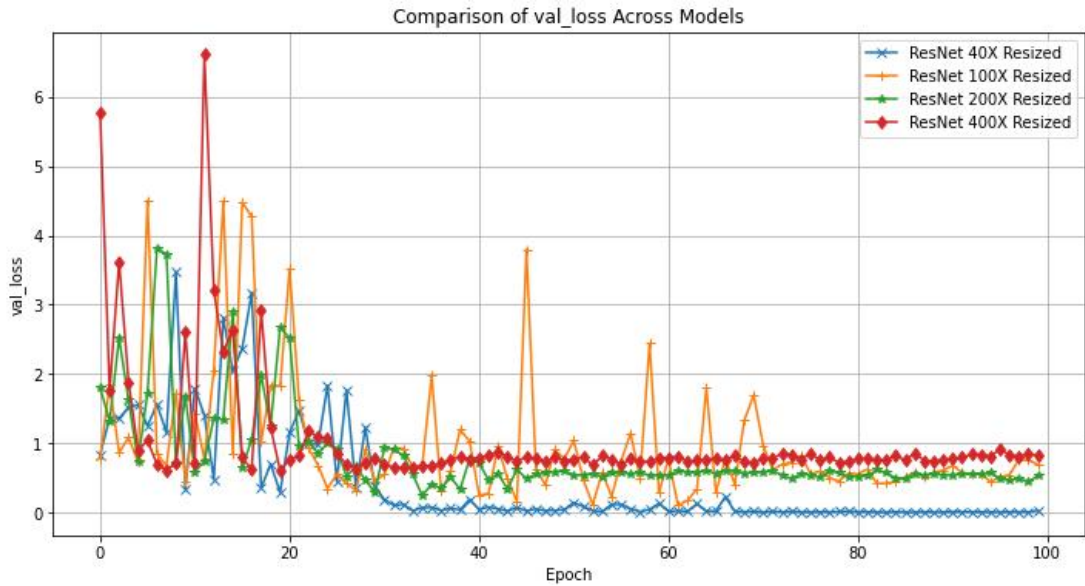


Figure 42: ResNet Validation Loss Comparison

4.4 Depthwise Network Training on 40X Magnification

Both prior structures performed well in diagnosing the BreakHis dataset at 40X magnification. However, the basic notion of stacking numerous Inception-ResNet blocks may result in a large increase in the number of training parameters. To overcome this, depthwise convolution was included in the experiment. This addition reduces the number of parameters and computational burden while maintaining the model's efficiency and effectiveness. This network serve as a experiment on how depthwise structured network performs on the dataset therefore foresees how this

network will affect the combined network. Architectures and results are illustrate within Figure 43 and Figure 44.

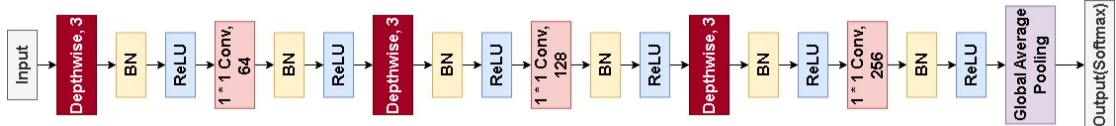
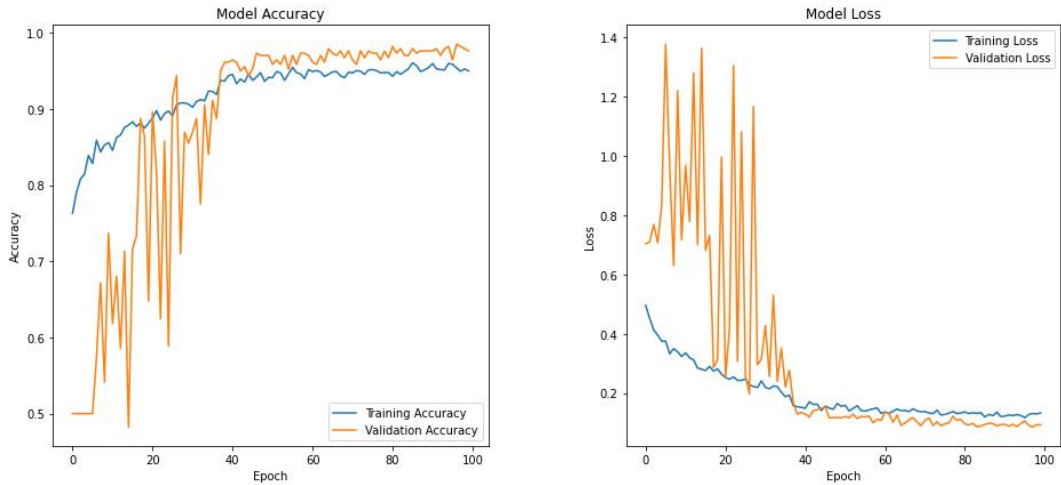


Figure 43: Depthwise CNN for experiment



a) Train Acc = 0.9500, Val Acc = 0.9763 b) Train Loss = 0.1334, Val Loss = 0.0929

Figure 44: a) and b) display Depthwise-CNN Train, Validation Accuracy and Loss on 40X Magnified Images

The depthwise convolution in 40X magnification network training has shown improved efficiency in parameter utilization and computation. The model maintains high training accuracy and mirrors this performance in validation metrics, a quality that Inception and ResNet structures may not fully achieve due to larger parameter sets. The stability in the validation loss curve indicates the depthwise network is less susceptible to fluctuations during learning, indicating a robust model capable of generalizing beyond training data without overfitting. This efficiency is expected to contribute to the integrated model, potentially playing a critical role in the training process and overall model performance.

4.5 Inception-ResNet (IR-Net) Training on 40X Magnification

To establish a foundational blueprint for the final model, we've constructed an initial Inception-ResNet model. This step aims to harness Inception's detailed feature extraction and ResNet's efficient backpropagation to create a robust structure. Testing

this model at 40X magnification will help assessing its training effectiveness and inform its influence on the final model's performance. Figure 45 and 46 represent the structure of Inception-ResNet, and Figure 47 illustrates the results training on the 40X magnified images.

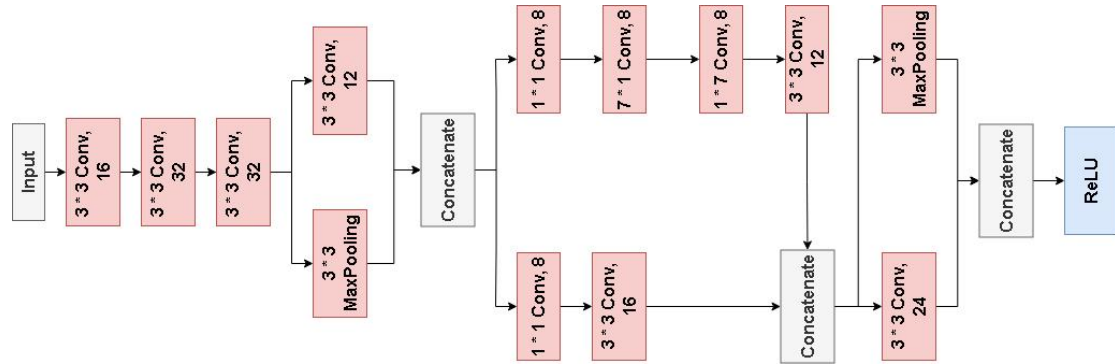
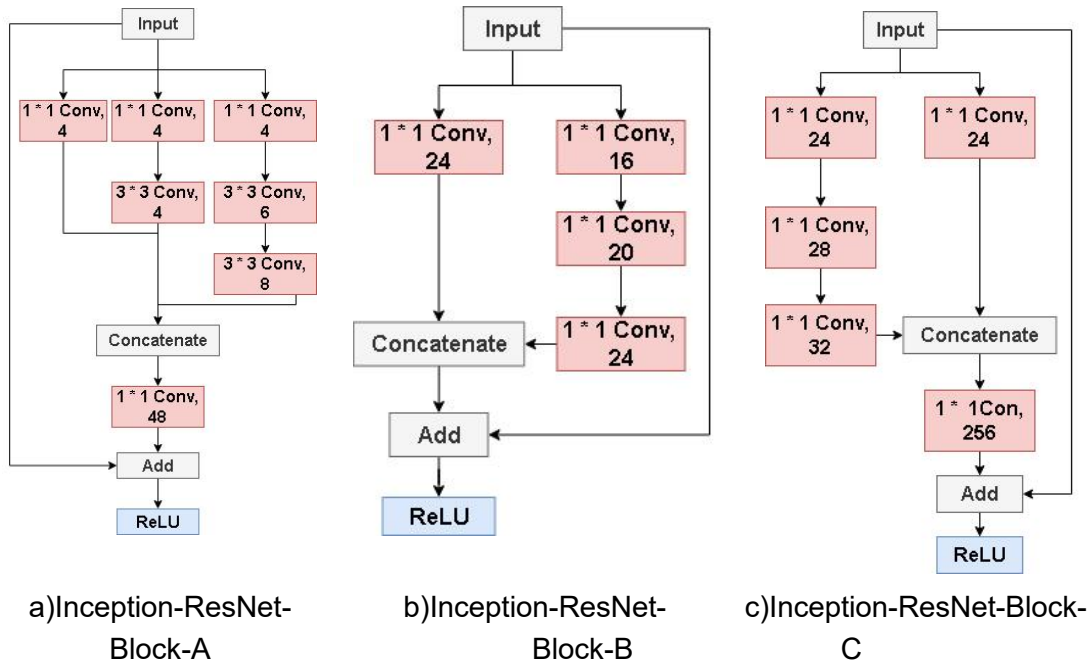
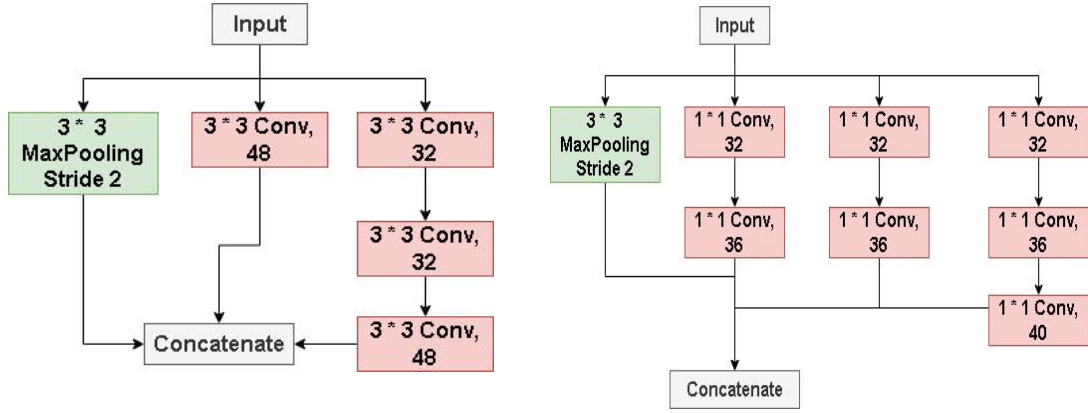


Figure 45: Inception-ResNet STEM block. This prototype model is the same as the prototype in chapter 3.

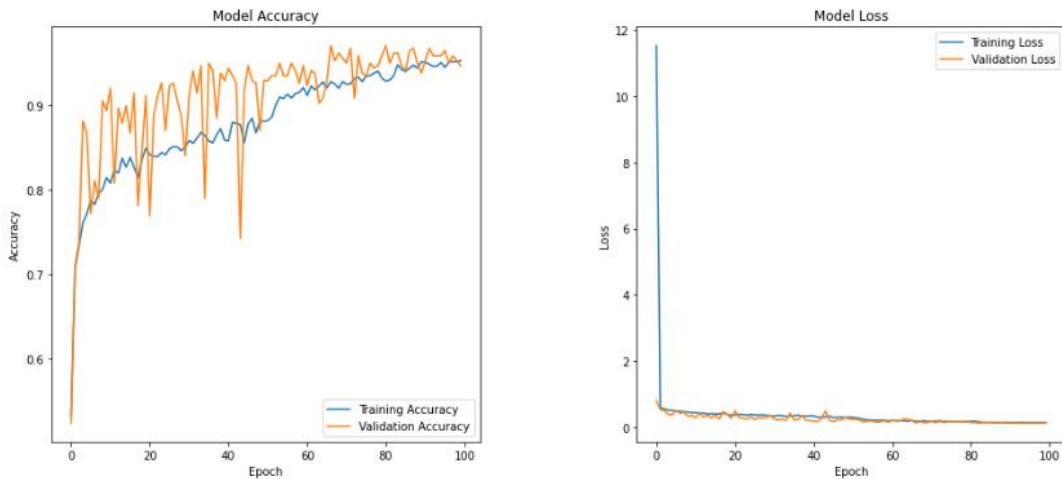




d) Inception-ResNet-Reduction-Block-A

e) Inception-ResNet-Reduction-Block-B

Figure 46: Inception-ResNet Structure for experiment



a) Train Acc = 0.9527, Val Acc = 0.9467

b) Train Loss = 0.1302, Val Loss = 0.1354

Figure 47: a) and b) display InceptionResNet Train, Validation Accuracy and Loss on 40X

Magnified BreakHis Resized images

The Inception-ResNet model trained at 40X magnification shows promising results, with rapid convergence in both training and validation accuracy. The model's loss graph shows a sharp decrease and plateau, indicating it's not overfitting and minimizing loss effectively. The model's stability at high values is crucial for clinical applicability, ensuring reliable diagnoses. The fusion of these architectures potentially primes the final model for robust performance.

4.6 Depthwise-Inception-ResNet (DIR-Net) Training on 40X Magnification

A unified model, DIR-NET, has been developed, introducing depthwise convolutional layers to the Inception-ResNet framework, aiming to add complexity without increasing computational load. The goal is to maintain a deep network design while

achieving an efficient training process. Figures 48 to 50 illustrate the modified Inception-ResNet block A and the DIR model along with the results.

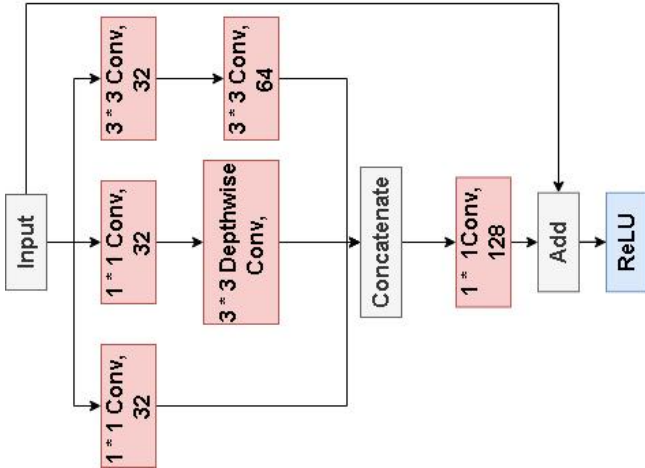


Figure 48: Depthwise-Inception-ResNet Block A

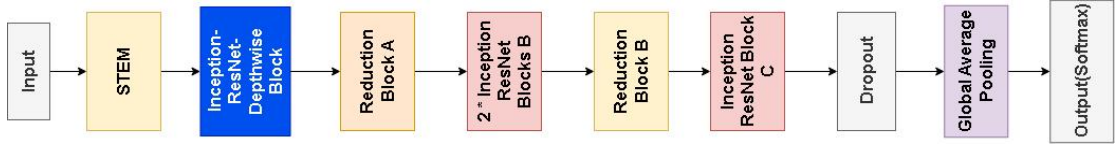


Figure 49: DIR model overview. Rest of the blocks remain the same as in

Inception-ResNet in 4.5

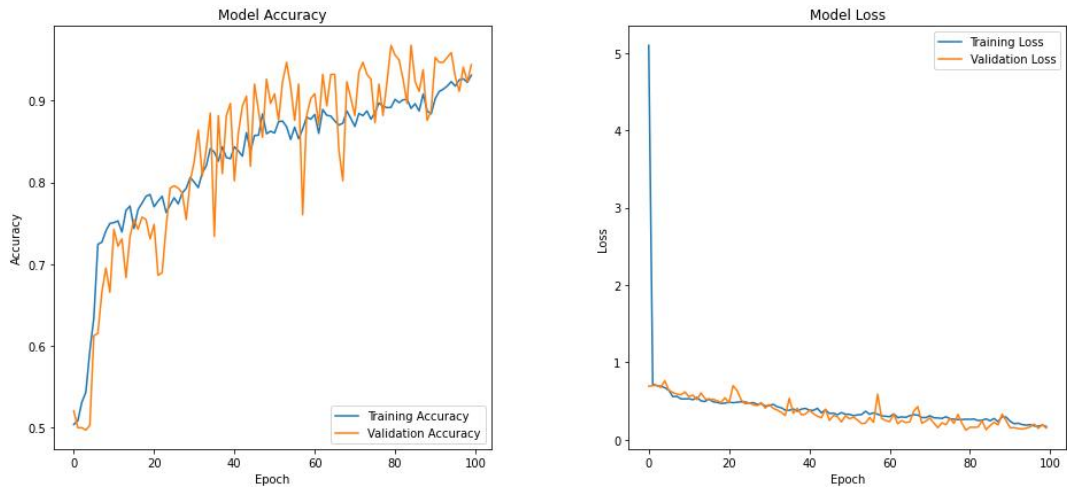


Figure 50: a) and b) demonstrate Depthwise-Inception-ResNet Train, Validation Accuracy and Loss on 40X Magnified Images

The DIR-Net trained on 40X magnification shows a positive trend in learning, with steady increases in model accuracy and a decrease in loss over epochs. Both training and validation accuracies show an upward trajectory, indicating effective learning.

However, fluctuations in validation accuracy suggest room for improvement in model stability. These fluctuations may be due to the model responding to complex patterns or sensitivity to validation set specificities. Integrating an attention mechanism in subsequent iterations could address these oscillations, focusing on salient input data, reducing performance variance, and mitigating underfitting by leveraging more informative features.

4.7 DIRA-Net Training on 40X Magnification

This part added the attention mechanism into the STEM block of the DIR-Net and while maintaining other blocks same as they were in [4.5 and 4.6](#). Following Figure 51 and Figure 52 represent the modification which will be the final structure of STEM block as mentioned in Chapter 3, and Figure 53 depicts the results for the initial DIRA-net.

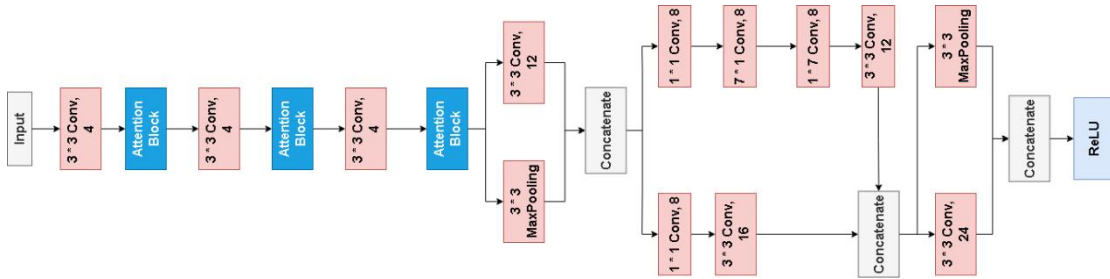


Figure 51: STEM Block with attention mechanism

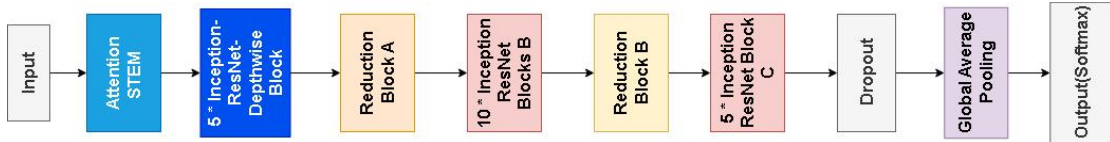
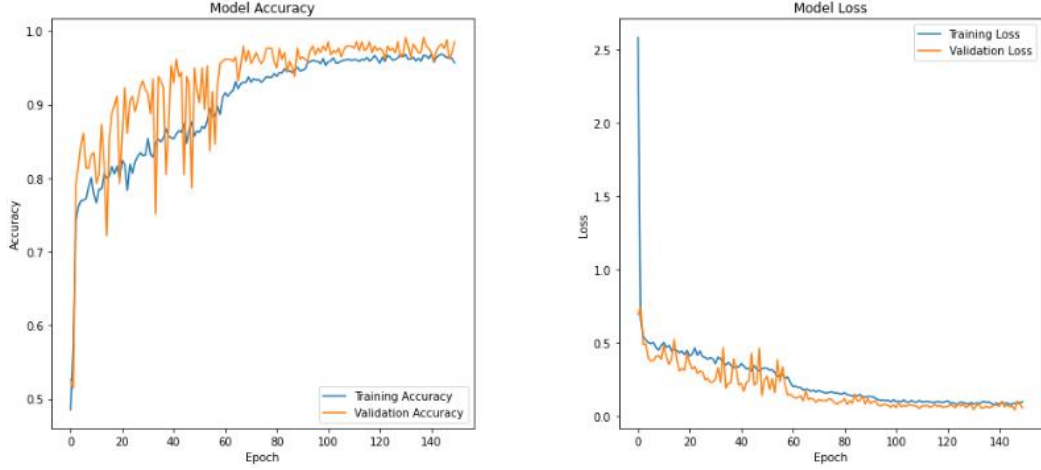


Figure 52: Initial DIRA-Net (With DIR-Block used 5 times, IR Block B and C used 10

and 5 times respectively)

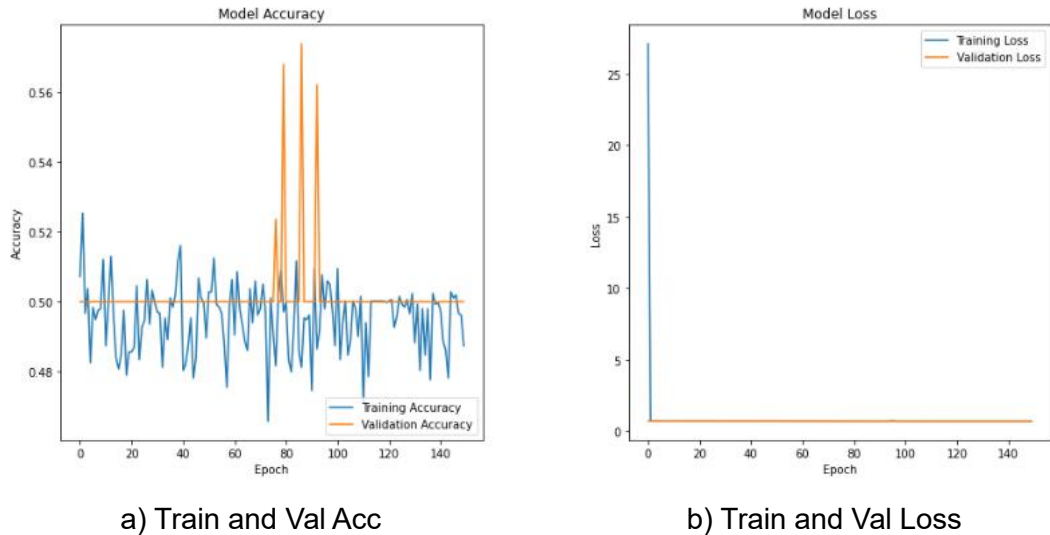


a) Train Acc = 0.9567, Val Acc = 0.9852 b) Train Loss = 0.1005, Val Loss = 0.0570

Figure 53: a) and b) demonstrates the model accuracy and loss

4.8 CLAHE Experiment

After implementing the original DIRA-Net model, it is vital to determine whether the color of the picture affects performance, therefore CLAHE images were compared to earlier images, and the findings are shown in Figure 54.



a) Train and Val Acc

b) Train and Val Loss

Figure 54: CLAHE Test Results

The DIRA-Net model's performance was evaluated, finding that CLAHE-enhanced images had suboptimal accuracy, suggesting distortion of information. Standard RGB images performed better, highlighting the importance of color in maintaining diagnostic accuracy. Therefore, CLAHE color alterations were excluded.

4.9 Model Evolution Summary

Table 5 displays the training results throughout the evolution of model from the first

single model to the initial version of the proposed model before fine tune.

Magnification	Magnification & Size	Validation	Validation	
		Accuracy	Loss	
Individual				
Raw Images				
InceptionNet	40X	0.9497	0.1362	
	100X	0.8323	0.3980	
	200X	0.9005	0.3123	
	400X	0.7782	0.8079	
Resized: 224 * 224				
	40X	0.9438	0.1617	
	100x	0.8259	0.4495	
	200x	0.8241	0.4191	
	400x	0.7030	1.0301	
Individual				
Resize: 224*224				
ResNet	40X	0.9941	0.0298	
	100X	0.8956	0.6940	
	200X	0.8931	0.5330	
Depthwise-CNN	Resize: 224*224	0.9763	0.0929	
40X				
IR-Net	Resize: 224* 224	0.9467	0.1354	
40X				
DIR-Net	Resize:224*224	0.9438	0.1496	
40X				
DIRA-Net	Resize:224*224	0.9852	0.0570	
40X				

Table 5: Model Evolution Summary

4.10 Fine Tune

The fine-tuning step focuses on improving the model's architecture and hyperparameters to get the greatest potential performance. To vary the model's depth,

adjust the number of times of Depthwise Inception ResNet Blocks as well as Inception-ResNet Blocks B and C being used. Furthermore, fine-tuning will entail adjusting the dropout rates to avoid overfitting and building a learning rate scheduler for more effective training. Table 6 details the essential parameters in the preliminary version of the proposed model, establishing the framework for these fine-tuning modifications.

Batch Size	DIR-Bloc k	IR-Block Called	IR-Block -B Called	IR-Block -C Called	LR	Dropout	Epoch	Para
	Times	Times	Times					
32	5	10	5	0.01	0.5	150	486,321	

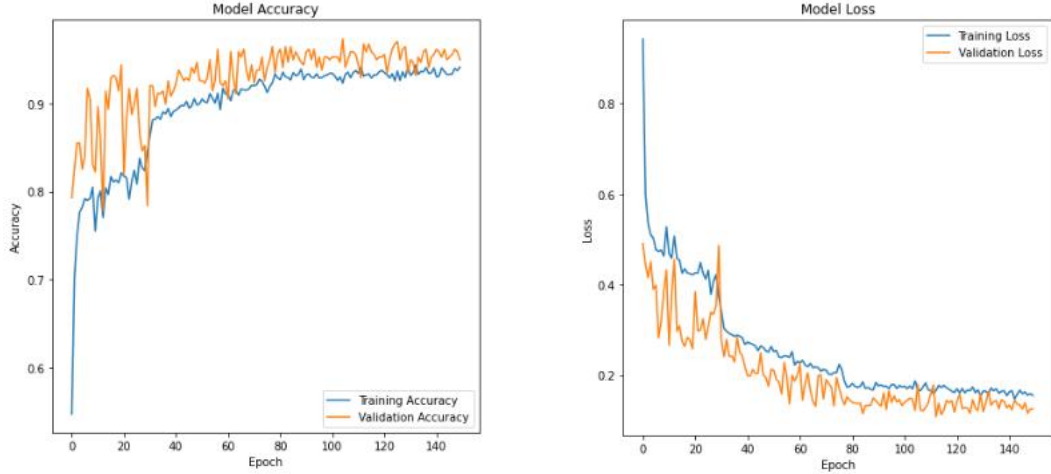
Table 6: Hyperparameters of the initial DIRA-Net

The results and details of hyperparameters of modifications are shown in the following graphs and tables, where Times is the number of times each of these three blocks were used.

First attempt of fine-tuning, as detailed in Figure 55 and Table 7, entailed reducing IR-Block B's frequency to eight and applying a dynamic learning rate reduction from 0.01. The diminished results, showcasing a minimal accuracy gap between validation and training only at the endpoint, indicate potential structural issues in the model, which may be too complex or simple for the given task. Subsequent steps will involve reinstating the original frequency of layer usage and examining the impact of batch size, filter number, and learning rate to discern their individual effects.

VN	BS	FN	Times	LR	Patience	Dropout	Epoch	L2
1	32	16	5,8,5	0.01	10	0.5	150	No

Table 7: Hyperparameters of model fine tune version 1



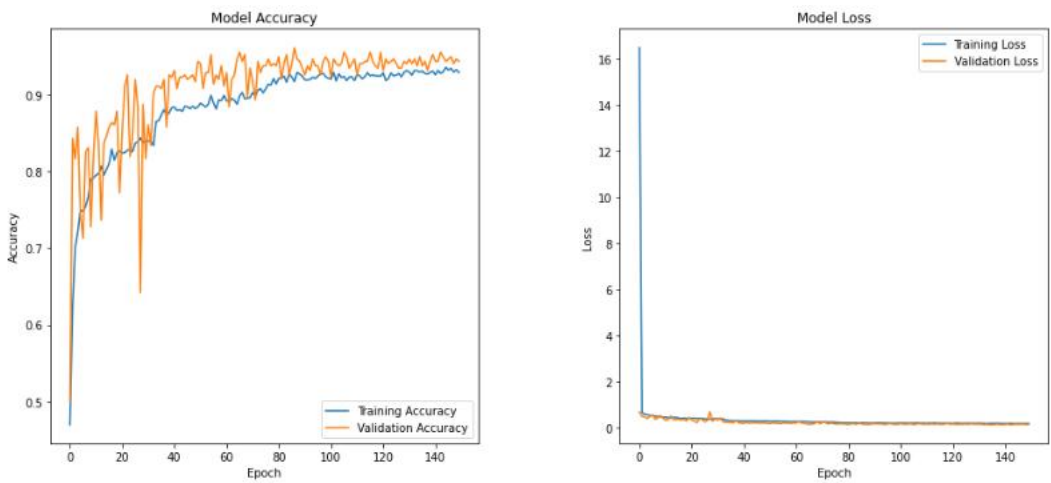
a) Train Acc = 0.9412, Val Acc = 0.9497 b) Train Loss = 0.1517, Val Loss = 0.1262

Figure 55: a) and b) are training results when DIR-Block is called 5 times, IR-Block-B is called 8 times, and IR-Block-C is called 5 times

As shown in Figure 56 and Table 8, by reducing the batch size to 16 and maintaining the frequency of each layer, it does not significantly resolve the underfitting problem. It indicates that batch size and filter numbers of STEM Block layers could not be the main effect of model performance which could be decreased afterwards to reduce parameters and maintain high accuracy. Additionally, model performance might still be limited by each part's usage, learning rate, dropout, and whether regularization is used.

VN	BS	FN	Times	LR	Patience	Dropout	Epoch	L2
2	16	8	5,10,5	0.01	10	0.5	150	No

Table 8: Hyperparameters of version 2



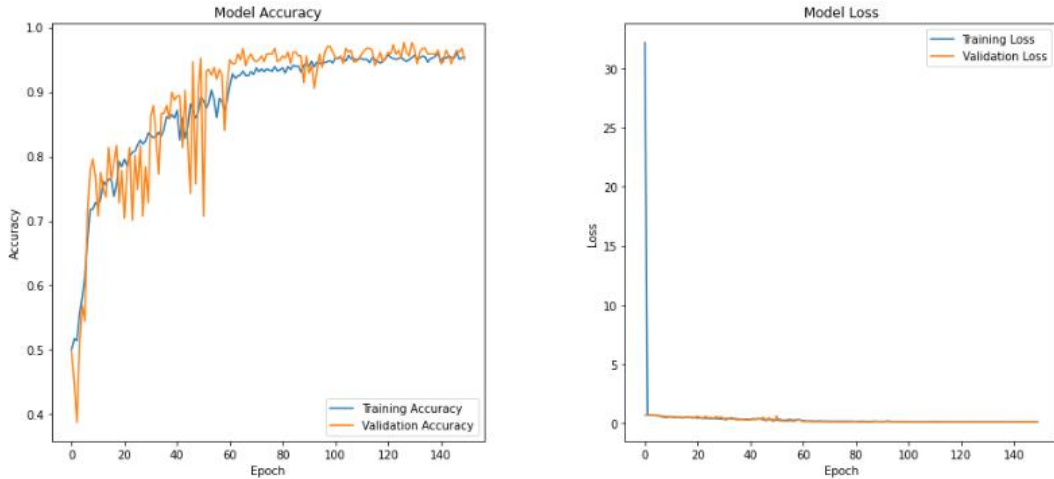
a) Train Acc = 0.9293, Val Acc = 0.9438 b) Train Loss = 0.1870, Val Loss = 0.1543

Figure 56: a) and b) training results when DIR-Block is called 5 times, IR-Block-B is called 10 times, and IR-Block-C is called 5 times with 16 Batch Size, with the first layer of STEM Block using 8 filters

Figure 57 and table 9 shows notable improvement with learning rate starting from 0.001. This suggests that the initial learning rate may have been high, and that lower starting point is more conducive for the model to effectively learn and properly converge.

VN	BS	FN	Times	LR	Patience	Dropout	Epoch	L2
3	32	8	5,10,5	0.001	10	0.5	150	No

Table 9: Hyperparameters for version 3



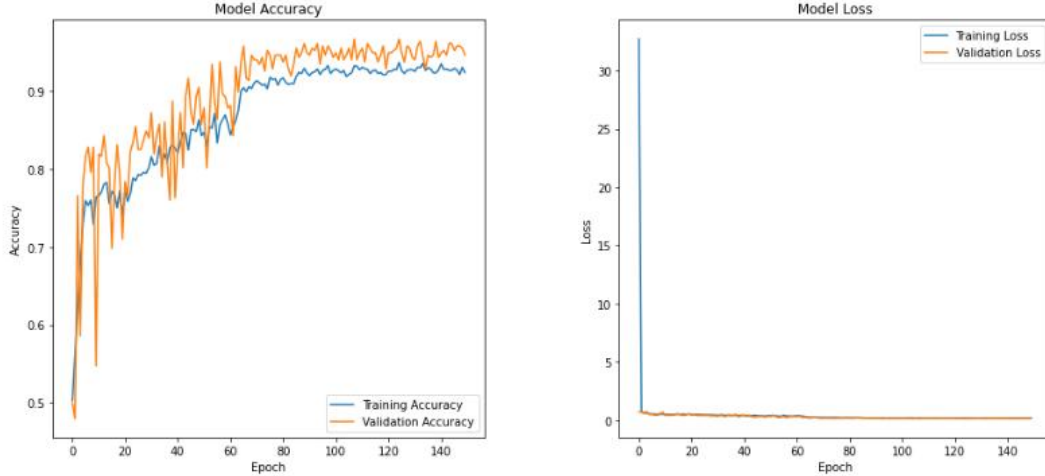
a) Train Acc = 0.9536, Val Acc = 0.9497 b) Train Loss = 0.1221, Val Loss = 0.1221

Figure 57: a) and b) demonstrate results of DIR-Block Called 5 times, IR-Block-B called 10 times, IR-Block-C called 5 times, batch size 32, with the first layer of attention stem block using 8 filters

In order to further optimize the model, regularization is added with reduction of filter numbers in STEM block in Table 10. However, the resulting underfitting in Figure 58 suggests that while regularization helps in controlling model complexity, the parameter tuning might have been too stringent which cannot capture enough patterns from the data.

VN	BS	FN	Times	LR	Patience	Dropout	Epoch	L2
4	32	4	5,10,5	0.001	10	0.5	150	Yes

Table 10: Hyperparameters of Version 4



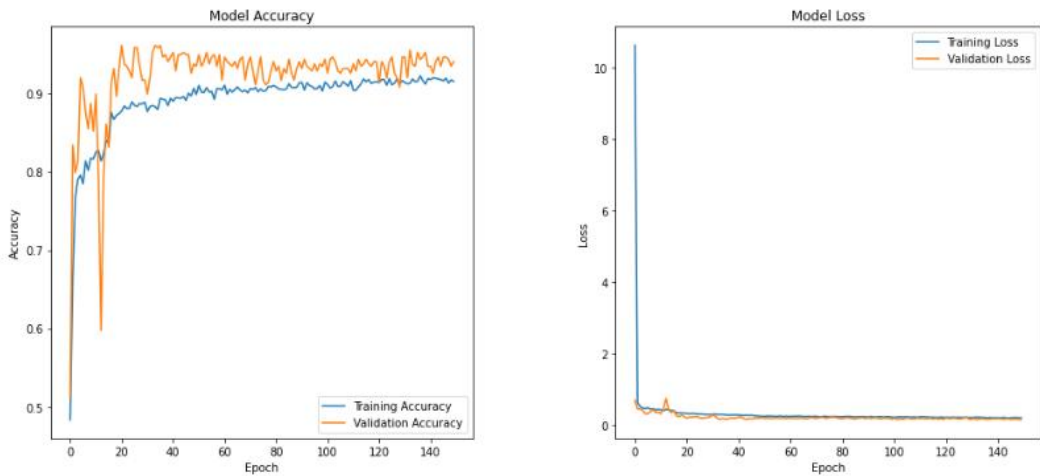
a) Train Acc = 0.9244, Val Acc = 0.9467 b) Train Loss = 0.2002, Val Loss = 0.1655

Figure 58: a) and b) illustrate results of DIR-Block Called 5 times, IR-Block-B called 10 times, IR-Block-C called 5 times. And added L2 regularization

Moving into the fifth modification, Figure 59 and Table 11 display an increase in IR-Block C frequency to address model's oversimplification from L2 regularization. It led to further underfitting, which hints that the mode might be more sensitive to block usage frequency.

VN	BS	FN	Times	LR	Patience	Dropout	Epoch	L2
5	32	4	5,10,7	0.001	10	0.4	150	Yes

Table 11: Hyperparameters of Version 5



a) Train Acc = 0.9156, Val Acc = 0.9408 b) Train Loss = 0.2133, Val Loss = 0.1582

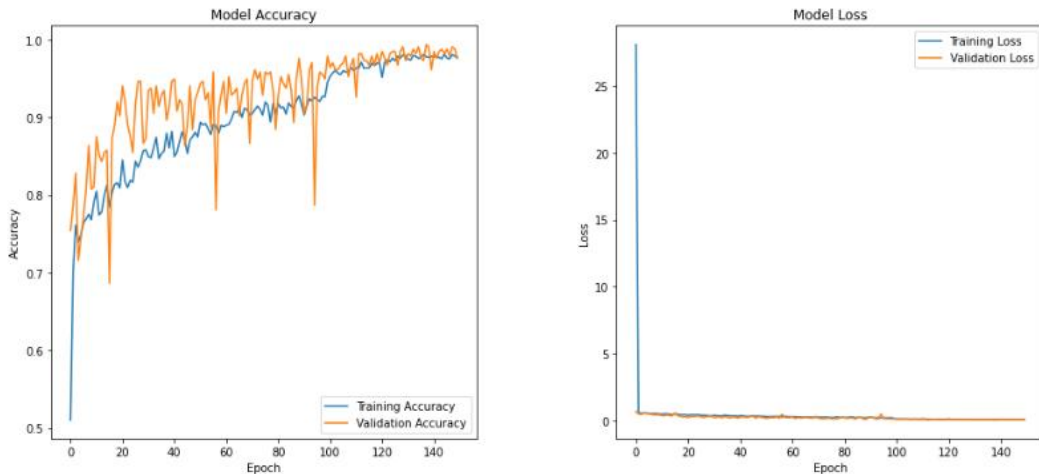
Figure 59: a) and b) display results of DIR-Block Called 5 times, IR-Block-B called 10 times, IR-Block-C called 6 times. And added L2 regularization

Few attempts of usage frequency were conducted, only the following three possess significant changes and could indicate the impact of blocks.

Looking into Figure 60 and Table 12, the obvious reduction of three blocks and a lower dropout rate had led to better model performance evidently through the smaller gap between train and validation accuracy and the lowering losses.

VN	BS	FN	Times	LR	Patience	Dropout	Epoch	L2
6	32	4	4,5,4	0.001	10	0.4	150	Yes

Table 12: Hyperparameters of Version 6



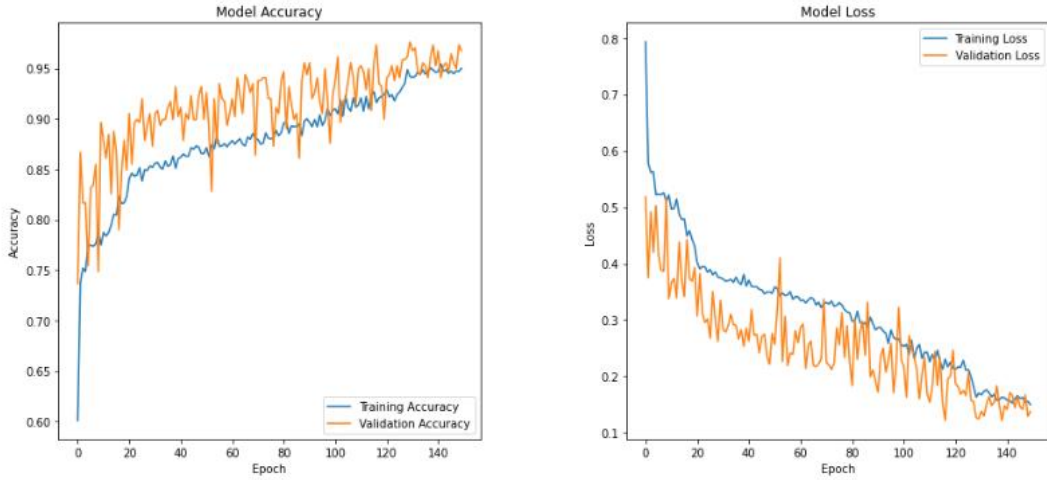
a) Train Acc = 0.9770, Val Acc = 0.9763 b) Train Loss = 0.0905, Val Loss = 0.0889

Figure 60: a) and b) are results of DIR-Block Called 4 times, IR-Block-B called 5 times, IR-Block-C called 4 times. And added L2 regularization

However, table 13 and figure 61 displayed an arresting underfitting while the IR-Block C usage frequency once again standout from the issue. This suggests that the overuse of IR-Block C indeed causes some levels of underfitting.

VN	BS	FN	Times	LR	Patience	Dropout	Epoch	L2
7	32	4	1,2,5	0.001	10	0.3	150	Yes

Table 13: Hyperparameters of Version 7



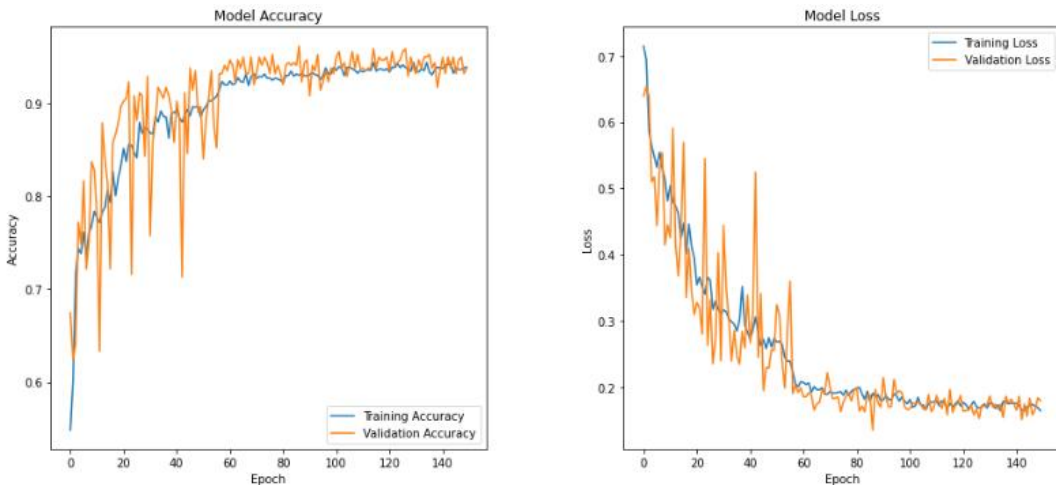
a) Train Acc = 0.9501, Val Acc = 0.9675 b) Train Loss = 0.1500, Val Loss = 0.1380

Figure 61: a) and b) are results of DIR-Block Called 1 times, IR-Block-B called 2 times, IR-Block-C called 5 times. And added L2 regularization

According to table 14 and figure 62, performance of model had increased and underfitting were prominently resolved with an extreme reduction of the usage frequency which indicates that complexity of model was high due to the numbers of branches and layers within each block.

VN	BS	FN	Times	LR	Patience	Dropout	Epoch	L2
8	32	4	1,1,1	0.001	10	0.3	150	Yes

Table 14: Hyperparameters of Version 8



a) Train Acc = 0.9390, Val Acc = 0.9379 b) Train Loss = 0.1641, Val Loss = 0.1796

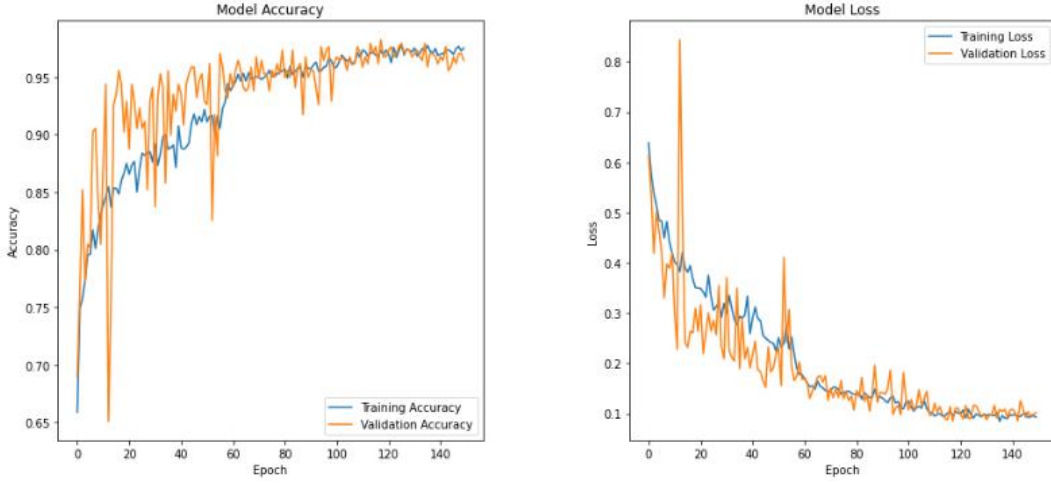
Figure 62: a) and b) show results of DIR-Block Called 1 times, IR-Block-B called 1 times, IR-Block-C called 1 times. And added L2 regularization

Finally, table 15 and figure 63 displayed the results of the last attempt, which perfectly

resolve the performance issue by adding layers into the model with the slight usage frequency increase of IR-Block B.

VN	BS	FN	Times	LR	Patience	Dropout	Epoch	L2
9 (Proposed)	32	4	1,2,1	0.001	10	0.3	150	Yes

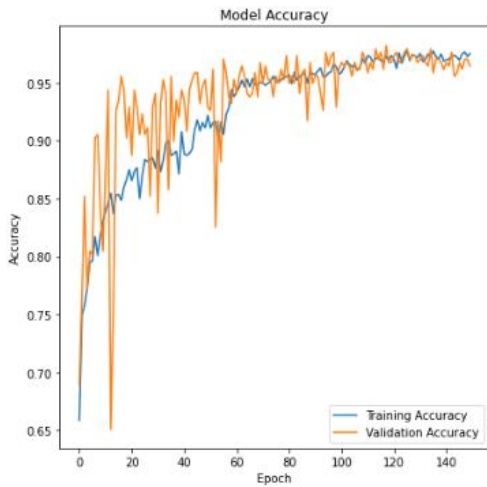
Table 15: Hyperparameter of Proposed Version



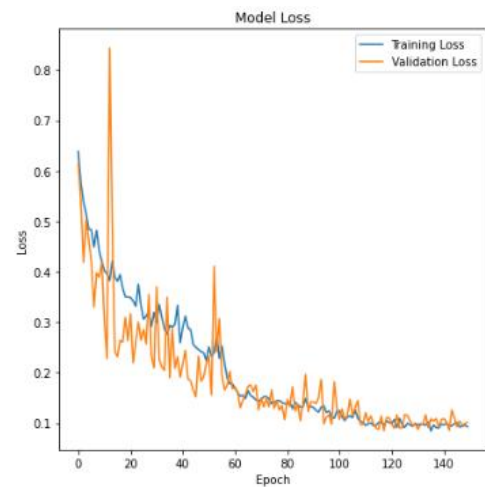
a) Train Acc = 0.9753, Val Acc = 0.9645 b) Train Loss = 0.0929, Val Loss = 0.1070

Figure 63: a) and b) demonstrate results of DIR-Block Called 1 times, IR-Block-B called 2 times, IR-Block-C called 1 times. And added L2 regularization

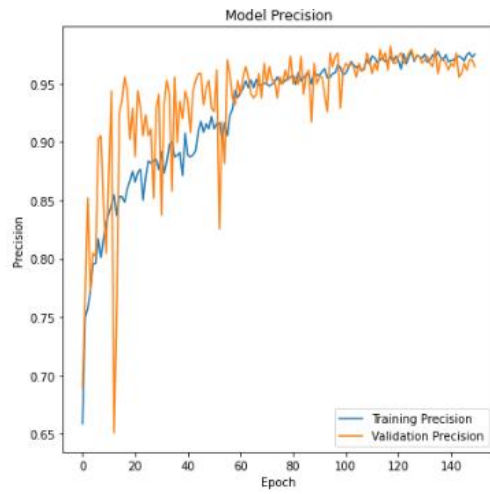
After fine-tuning, the model achieved a balance between structural complexity and performance, avoiding overfitting or underfitting. The consistency in loss and accuracy graphs confirmed its competence. The final structure delivered commendable statistical metrics and proven capability in practical breast cancer classification scenarios. Figure 64 displays all the evaluation matrix of the proposed model. Table 16 summarizes the modified results and parameters in each round, where Acc, Loss, F1, Rec, Prec, Spec, Para represents Accuracy, Loss, F1-Score, Recall, Precision, Specificity, Area Under Curve, Total Parameters, which are all statistics of validation. And Table 16 summarized the fine-tune process.



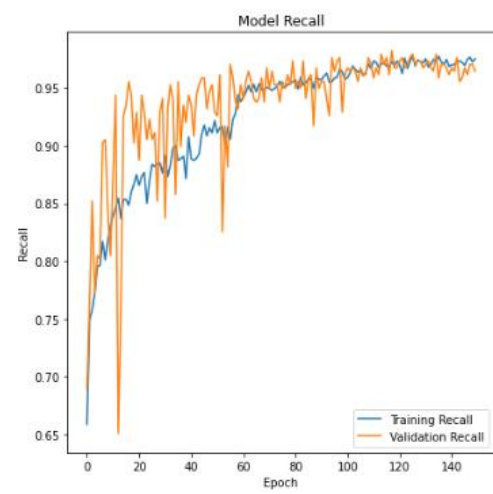
a) Train Acc = 0.9753, Val Acc = 0.9645



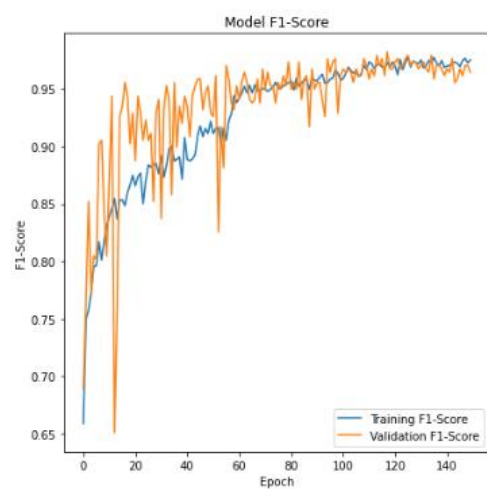
b) Train Loss = 0.0929, Val Loss = 0.1070



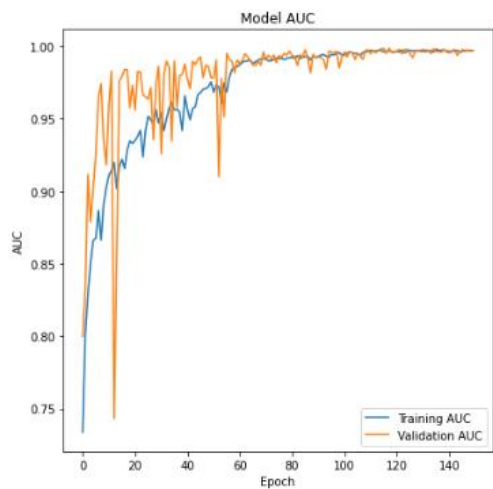
c) Train Prec = 0.9753, Val Prec = 0.9645



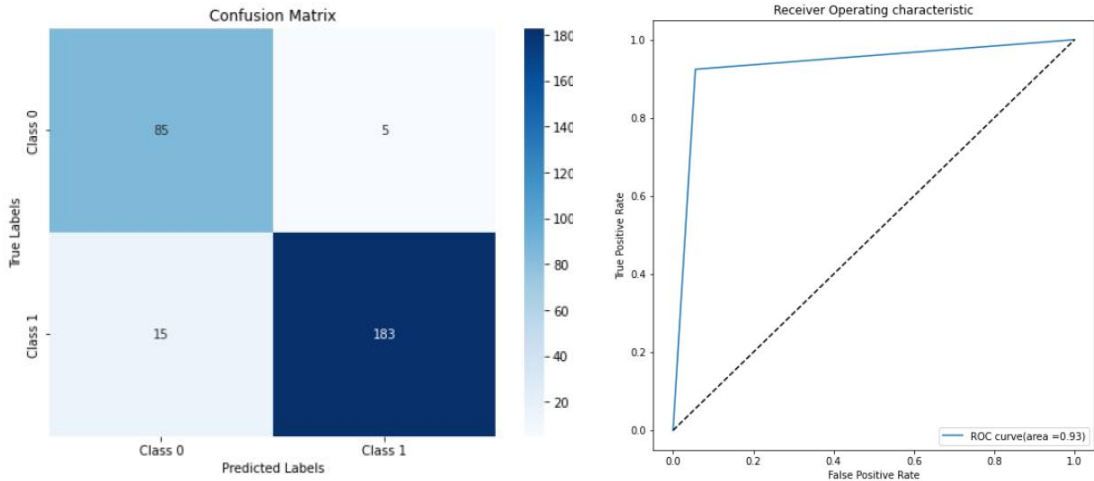
d) Train Recall= 0.9753, Val Recall= 0.9645



e)Train F1= 0.9753, Val F1= 0.9645



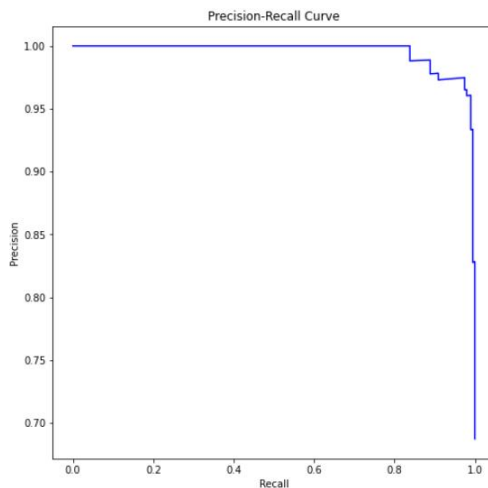
f) Train AUC= 0.9968, Val AUC= 0.9968



g) Confusion Matrix, where Class 0 and

h) ROC Curve Graph AUC =0.93

Class 1 represents Benign and Malignant



i) Precision-Recall Curve

Figure 64: a) to i) represents all the matrix of the proposed model, as micro-f1 score, micro-precision, micro-recall has the same calculation in binary which results in similar graph.

VN	Acc (%)	Loss (%)	F1 (%)	Rec (%)	Prec (%)	Spec (%)	AUC (%)	Para
1	94.97	12.62	93.98	95.58	91.24	92.94	94	448,121
2	94.38	15.43	90.94	92.38	94.41	91.20	92	490,033
3	94.97	12.21	89.84	91.32	94.87	90.21	91	505,821
4	94.67	16.55	91.17	93.45	94.67	90.24	90	505,812
5	94.08	8.89	93.73	92.24	94.46	91.26	91	1,152,825

6	97.63	8.90	93.26	94.41	97.62	93.40	94	372,989
7	96.75	13.80	94.30	96.48	96.75	92.13	94	703,533
8	93.79	17.96	90.67	93.96	93.79	87.64	91	273,617
9	96.45	10.70	96.45	92.24	96.45	94.44	93	313,597
(PROPOSED)								

Table 16: Fine tune process and results summary

4.11 Comparison Analysis

Table 17 and 18 below shows the comparison analysis of the proposed model and previous works, figure 65 and 66 displays the comparison with pre-models.

Authors	Datasets	Acc (%)	Loss (%)	AUC (%)	F1 (%)	Sen (%)	Spec (%)	Prec (%)
Hirra et al. [1]	Histopathology images	86	15	X	X	87.9	84	X
Sahu et al. [9]	Mini-DDSM	99.17	X	99	99	99.0	99.5	X
	Ultrasound Images (BUSI)	96.92	X	96	98	98.8	94.62	X
Liang and Meng [19]	BreakHis	95.50	X	X	X	X	X	X
Alkhaldi and Salari [20]	Invasive-Ductal-Carcinoma (IDC)	92.87	X	X	90	85.9	90.98	93.6
Xu et al. [21]	BreakHis	98.0	X	X	X	X	X	X
Wu et al. [22]	224,426 mammography	X	X	89	X	X	X	X
Chougrad et al. [23]	DDSM	97.35	X	98	X	X	X	X
	INbreast	95.50	X	97	X	X	X	X
	BCDR	96.67	X	96	X	X	X	X
Yu et al. [24]	INbreast mini-DDSM (Merged)	96.11	X	X	X	92.8	98.55	95.7
Arya and Saha [25]	1,980 patients' breast cancer data	90.2	X	93	X	X	X	X

Chattopadhyay et al., [26]	BreakHis	97.12	X	X	96	96	X	97
Addo et al., [27]	BreakHis	99.15	X	X	X	X	X	X
Proposed	BreakHis	96.45	10.07	93	92	92	94	97

Table 17: Comparison Analysis with Previous Works

Based on Table 17, the proposed model had reached ideal results comparing to previous researches. It is noticeable that the accuracy had surpassed some of those using histopathological images and reached similar performance as others. Moreover, other evaluation statistics such as AUC, sensitivity, specificity F1-Score and precision were also either higher or similar to previous models. Moving on, a comparison with two popular pre-trained model were conducted, and results are provided in Figure 65, Figure 66 and Table 18.

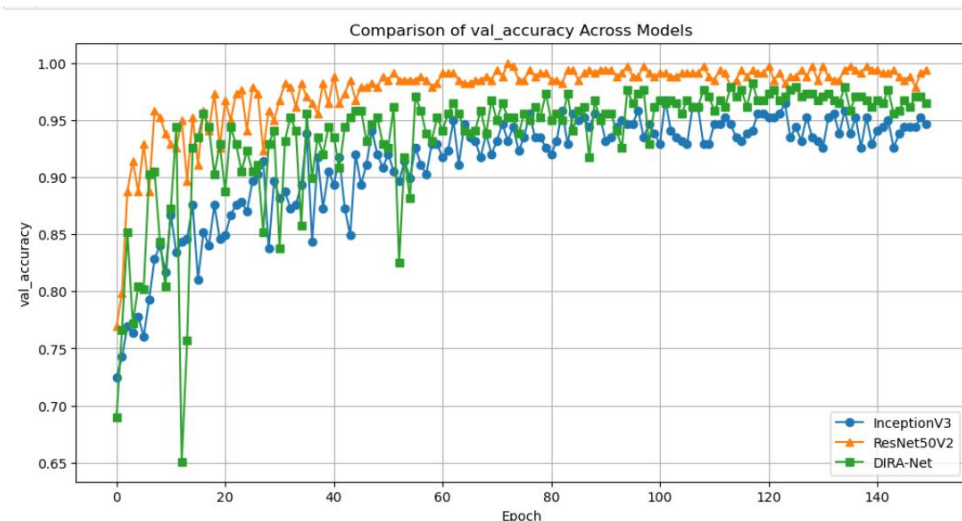


Figure 65: DIRA-Net Validation Accuracy Comparison with Pre-trained Models

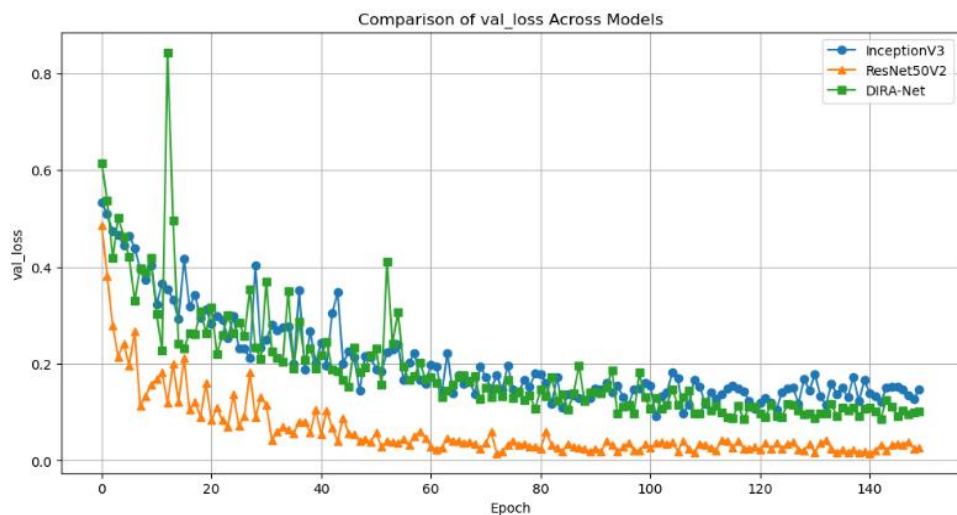


Figure 66: DIRA-Net Validation Loss Comparison with Pre-trained Models

Model	Acc (%)	Loss (%)	F1 (%)	Rec (%)	Prec (%)	Spec (%)	AUC (%)	Para
ResNet50V2 -Pretrained	99.41	2.57	94.18	98.42	99.41	87.47	93	24,614,914
InceptionV3- Pretrained	94.67	14.70	88.69	94.52	90.67	81.31	88	22,852,898
DIRA-Net	96.45	10.17	96.45	96.45	93.09	94.44	93	313,597

Table 18: Results Comparison of DIRA-Net with Pre-trained Models

In comparison with existing pre-trained models, DIRA-Net not only matches their accuracy levels but also ensures higher efficiency with far fewer parameters, as demonstrated in the tables. This underlines the advantages of the proposed model, showcasing its ability to achieve optimal performance with a more compact and efficient architecture.

4.12 Model Visualization

Figure 67 and 68 visualize the focus point of the model on images which involved using both SHAP and Grad-CAM.

SHAP is a method that enhances interpretability of machine learning-based equalizers, especially in short-reach intensity modulation and direct detection systems. It visualizes and analyzes trained equalizers, reducing feature count without compromising performance, and offers a universal technique for system optimization and feature selection [33].

In SHAP analysis, red represents features that influence the model's prediction toward a specific class, while blue indicates features that contradict it. Using Figure 64 as an example, the first image shows predominantly blue in the 'benign' part and red in the malignant section of the heatmap, indicating a malignant forecast. In the second figure, the 'benign' part has larger red area, whereas malignant section has wider blue area, indicating a benign prediction.

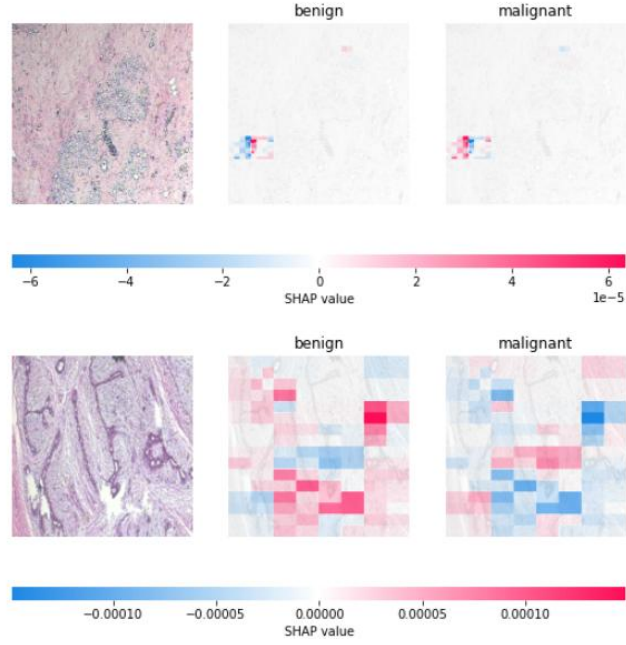


Figure 67: SHAP Visualization

Grad-CAM is a technique that visualizes Convolutional Neural Networks (CNNs) by highlighting localizations in images which enhances the interpretability of the model and extracts important variables [34]. How it works is that, the more blue the area is, the more focus the model is.

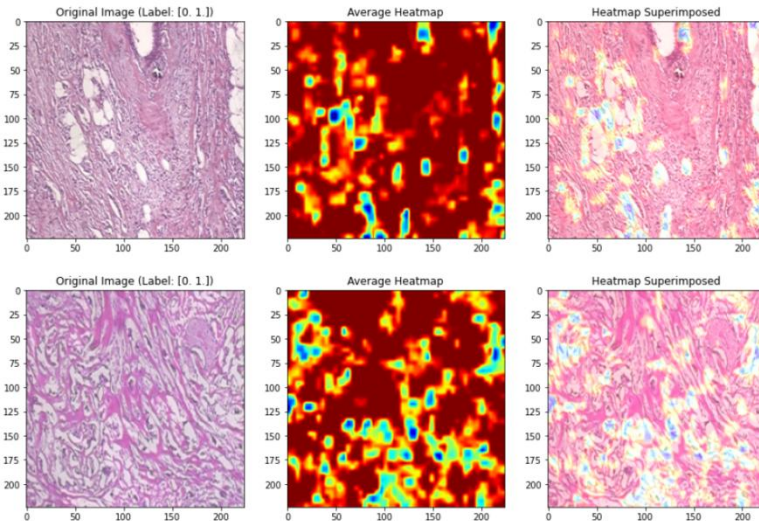


Figure 68: Grad-CAM Visualization

4.13 Model Deployment

The provided figures showcase the deployment website for our proposed model. On the homepage, users can find essential details and links to the breast cancer dataset. The "Get Diagnosis" button navigates users to the diagnostic page, where, upon scrolling down, one can find a description of the dataset accompanied by a link to its

Kaggle source. This link directs users to the detailed data source as depicted in Figures 69 and Figure 70.



Figure 69: Main Page

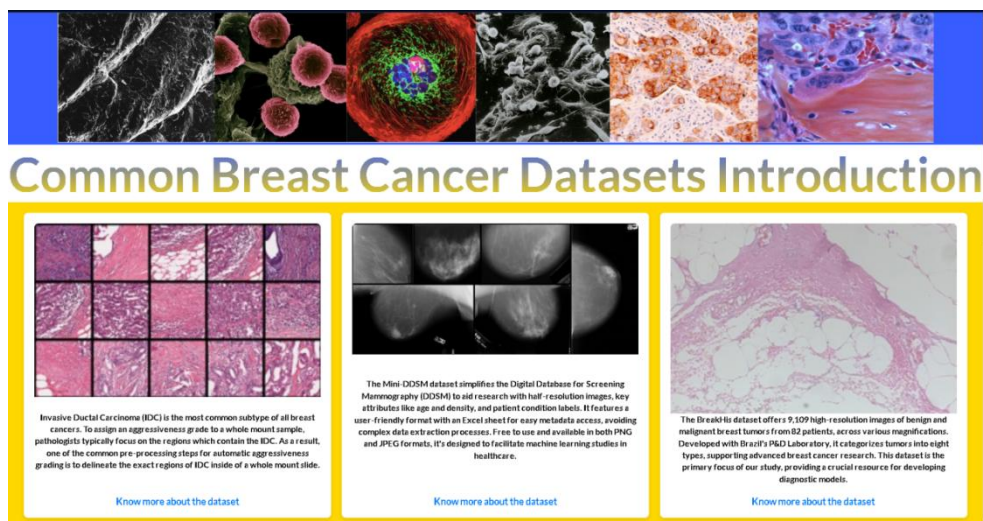


Figure 70: Dataset Introduction Cards

The diagnosis page features an intuitive drag-and-drop area for image uploads, and upon submitting an image with the "Get Diagnose" button, the page presents the classification results. For instance, as illustrated in Figure 71 and Figure 73, The system uses BreakHis dataset images to determine benign or malignant cases, with a bar chart indicating the model's confidence in the prediction, with green bars representing benign cases and red bars representing malignancy.

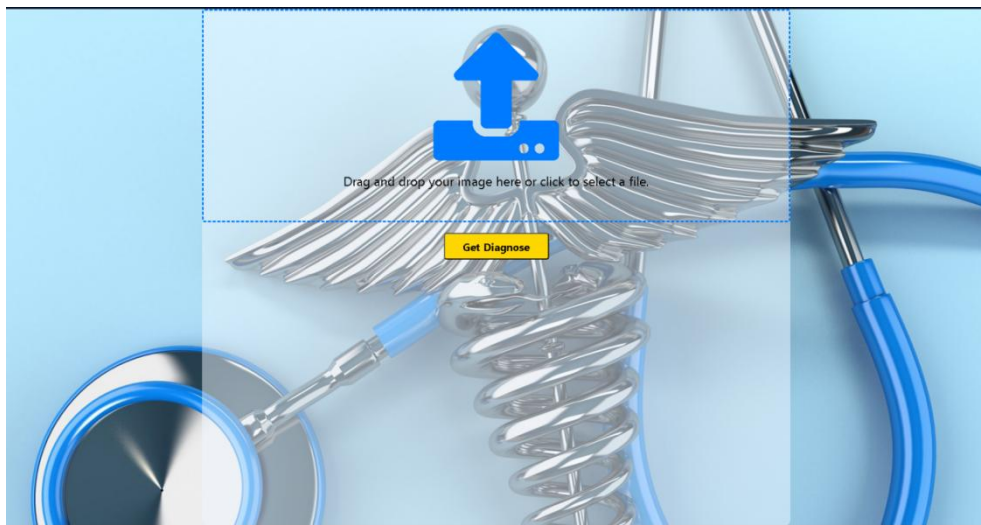


Figure 71: Diagnosis Page before Diagnosis

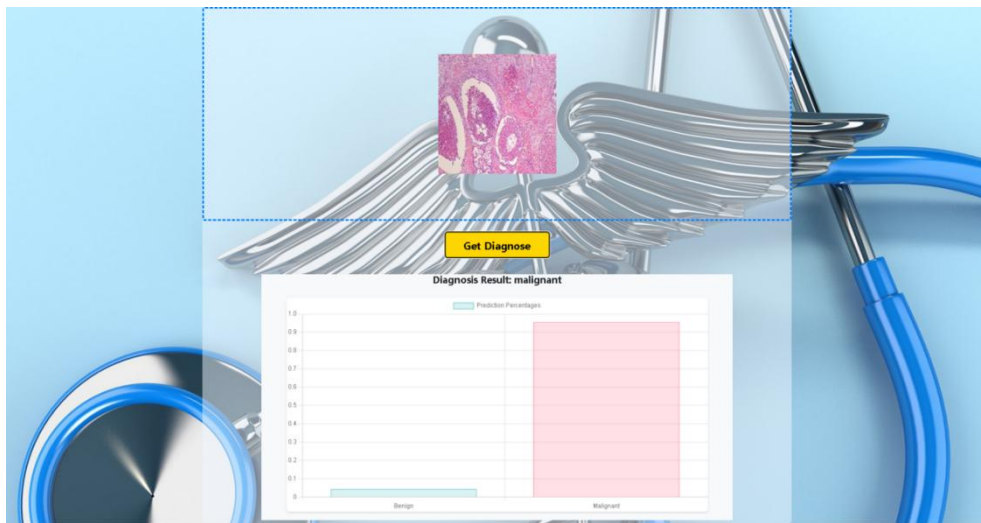


Figure 72: Malignant Diagnosis

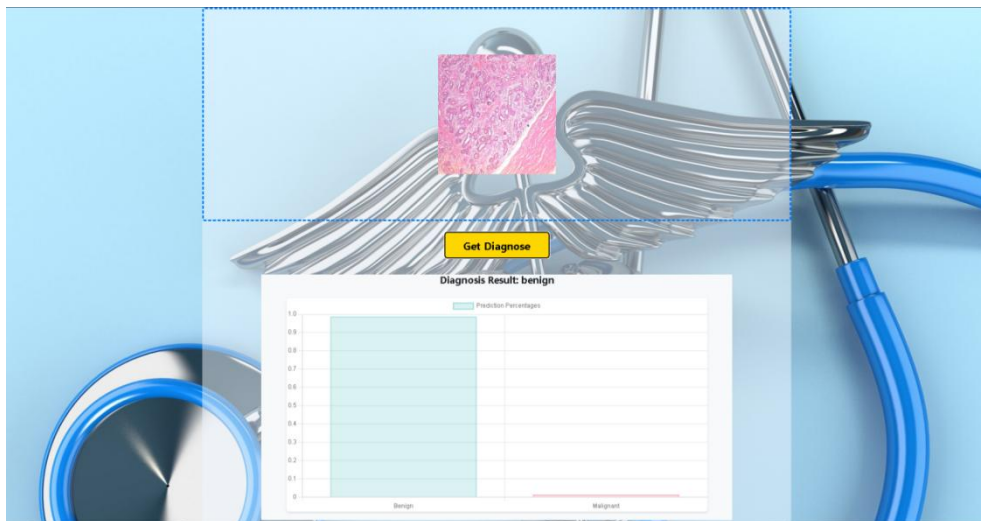


Figure 73: Benign Diagnosis

Chapter 5 Project Management

5.1 Activities

Phase	Task	Status
1-1	Conduct Breast Cancer Diagnosis Research	Complete
1-2	Identify and Narrow issues	Complete
1-3	Dig into solutions of deep learning method for breast cancer diagnosis	Complete
1-4	Study classification methods and models	Complete
2-1	Research on breast cancer diagnosis specifically in CNNs	Complete
2-2	Study six CNN models and relevant programming methods	Complete
2-3	Understand evaluation methods of CNNs	Complete
2-4	Investigate mechanisms to improve models and performances	Complete
3-1	Gather 1 to 3 datasets from Kaggle and select one suitable dataset	Complete
3-2	Complete basic data separation and preprocessing	Complete
3-3	Test the processed data on pre-trained models	Complete
4-1	Construct models with different combination of different mechanisms	Complete
4-2	Train the different combinations of model on the dataset	Complete
4-3	Conduct selection of mechanisms based on the training results	Complete
4-4	Sort out the experiments process and start fine-tuning	Complete
5-1	Compare the fine-tuned model with original final model and other existing model	Complete
5-2	Deploy the model with website application	Complete
5-3	Finish the final report, deployment and presentation preparation	Complete

Table 19: Activities of the Project

5.1.1 Schedule

The schedule is shown in Table 20.

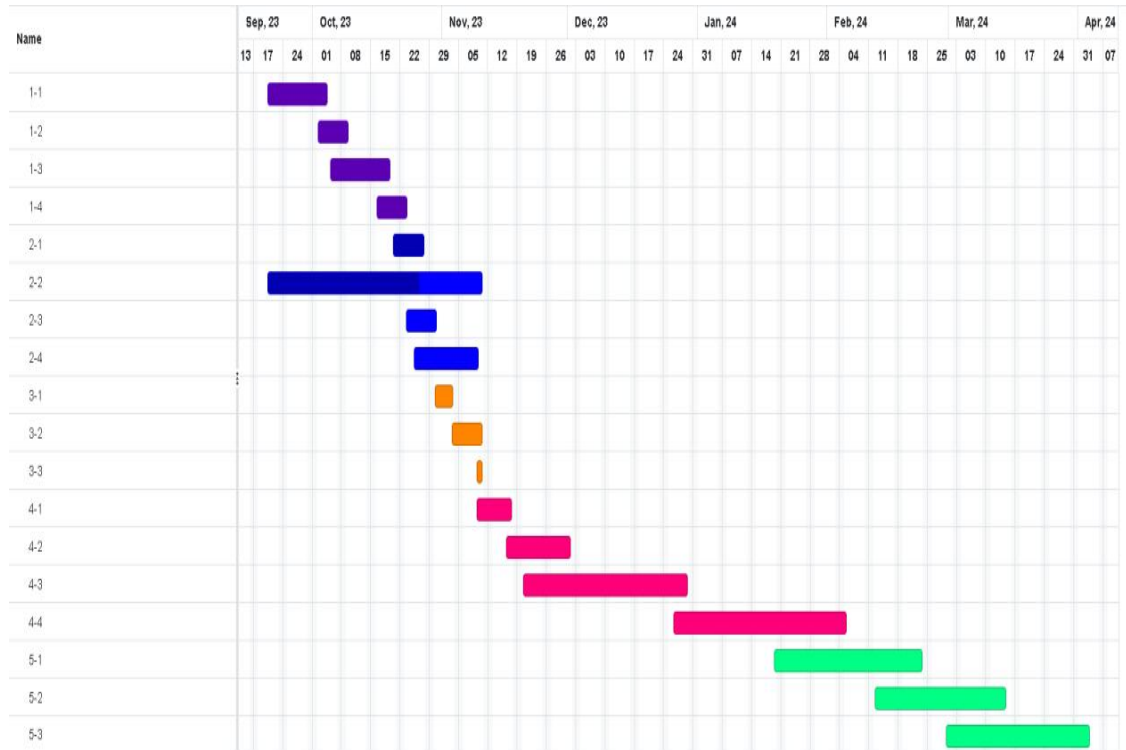


Table 20: Gantt Graph

5.1.2 Project Version Management

To manage the different versions of codes modification, I plan to use Github as the version management tools for keeping code updated and secure.

URL is as follow: <https://github.com/Vio1etV/Final Year Project>

Version Number	Code Name	Content	Results
1	Initial experiment models	Experiments of Inception-Net, Res-Net, Depthwise-Net. Raw and preprocessed images.	Training results, CSV files of training, initial model design diagrams
2	Combination of models	Experiments of IR-Net, DIR-Net, initial DIRA-Net.	Training results CSV file of training, initial design diagrams, .h5 file of initial DIRA-Net.
3	DIRA-Net fine tune	All the .ipynb files of each fine-tuned model.	.h5 files of DIRA-Net, training results,

			Model verification files
4	Model deployment	The web-application program where the model can be added. Model .h5 file	Web application and model .h5 files

Table 21: Version Control Progress

5.1.3 Project Data Management

- A. All files including datasets, model codes, references, weekly reports and all sorts will be replicated into three copies for fail safe, one on local computer, one on hard drive, one on github.
- B. Upload the project to github for every modification, synchronize latest version.

Following are documents of the Project for uploading and synchronization:

1. Reports (Weekly, Proposal, Progress, Final) & Presentation PPT
2. CNN model diagram
3. References
4. Datasets Link
5. Model evaluation documents
6. CNN model codes (Different versions)
7. Model Deployment Codes

5.1.4 Project Deliverable

- A. The project proposal
- B. Weekly report
- C. Progress Report
- D. Final Project Report
- E. Project codes (Model codes & Deployment Codes)
- F. Project presentation slides
- G. Project Presentation
- H. Links(Datasets and Github)

5.2 Risk Analysis

Table 22 displays the analyzed risks during the project progress.

Risk ID	Potential Risk	Cause ID	Potential Causes	Severity	Likelihood	Risk	Mitigation ID	Mitigation
R 1.1	Loss of Project Data	C 1.1.1	Poor version Control	4	1	4	M1.1.1	Regularly update project to cloud
			Physical Hardware Failure	4	1	4	M1.1.2	Hardware Check & Backup
R 1.2	Memory Leakage	C 1.2.1	Model training exceeds the hardware ability	4	3	12	M1.2.1	Use cloud service
			C 1.3.1	2	4	8	M1.3.1	Augmentation & Upsampling
R 1.3	Model training issues	C 1.3.2	Data imbalance					
			Low data quality			4	M1.3.2	Find trusted source on kaggle
R 1.4	Software issues	C 1.4.1	Virtual environment error	4	1	4	M1.4.1	Keep Virtual Environment Clean
			C 2.1.1	3	1	3	M2.1.1	Keep healthy
R 2.1	Miss deadline	C 1.3.2	Poor time management					

Table 22: Risk Analysis

5.3 Professional Issues

In the course of this project's development, it is critical to address a wide spectrum of legal, social, ethical, and environmental concerns. This involves obeying the professional standards set forth by institutions like ACM(Association for Computing Machinery) and the BCS (The British Computer Society).

Legal: Legal issues surrounding the use of deep learning technologies in breast cancer diagnosis are influenced by strict privacy standards like HIPAA and GDPR.

These protocols govern the handling of sensitive patient information, including data anonymization and encryption. Legal elements include liability for diagnostic accuracy and intellectual property, ensuring that models respect all parties' legal rights during development, use, and sharing.

Social: Deep learning for breast cancer diagnosis necessitates a social approach, ensuring accessibility, reducing healthcare inequities, and fostering public confidence. Clear communication about benefits and drawbacks, managing relationships with diverse stakeholders, and encouraging an inclusive approach can improve health outcomes and public trust.

Ethical: Deep learning in breast cancer detection requires a cautious approach to ensure accurate and impartial diagnosis. This includes reducing biases, increasing openness, and ensuring informed consent. Patients should be informed about AI usage and consequences, and continuous ethical oversight is necessary to monitor and assess the technology's impact. This proactive governance ensures AI systems' integrity and trustworthiness in healthcare.

Environment: From an environmental perspective, the use of deep learning models in breast cancer detection has implications such as a significant energy consumption and carbon footprint due to the computational intensity of training these models. It's important to consider and strive for energy-efficient computing practices to mitigate this impact.

Using deep learning for breast cancer detection raises complex legal, social, ethical, and environmental considerations, including data privacy, equitable access, algorithmic fairness, transparency, and energy efficiency. If handled and operated properly, the aforementioned issues associated with using deep learning for breast cancer detection can be effectively mitigated.

Chapter 6 Conclusion

Throughout the project, a novel deep learning model, DIRA-Net, was successfully constructed and validated on BreakHis public dataset, aims to improve breast cancer diagnostic accuracy using histopathological pictures. The model combines Inception and ResNet architectures, depthwise convolutions and an attention mechanism, resulting in impressive performance metrics. DIRA-Net achieved an accuracy of 96.45%, an AUC of 93%, and an F1-Score of 92.14%, sensitivity of 92.42, specificity of 94.44% and overall 93.09% precision, indicating its potential as a critical tool in medical diagnostics.

The model's efficiency and accessibility, especially for real-time diagnostic applications, were enhanced by reducing the number of trainable parameters. The project's thorough methodology, including dataset preparation, model construction and various experiments, demonstrated its the effectiveness and practical usage. Comparative analysis further supported the model's unique features. It also illustrates how diverse deep learning techniques can be seamlessly integrated to improve diagnostic performance in medical imaging.

Although DIRA-Net has shown great performance in binary classification of breast cancer using histopathological images, its capacity to handle more complicated diagnostic situations is restricted. The model's multi-class classification proficiency now requires additional enhancement in order to properly discriminate between different forms of breast cancer on the BreakHis dataset. Improving this component of DIRA-Net would allow for more complete symptom analysis and precisely targeted treatment programs, making it more comprehensive and useful in clinical settings.

To enhance the robustness and utility of DIRA-Net, it is crucial to verify its performance on various public breast cancer datasets beyond BreakHis. This will improve diagnostic accuracy and clinical effect, expanding its influence on medical imaging and patient care in the breast cancer community. Future studies will enhance the model's generalizability and advance the development of more adaptable and effective diagnostic tools.

Reference

- [1] I. Hirra *et al.*, "Breast Cancer Classification From Histopathological Images Using Patch-Based Deep Learning Modeling," *IEEE Access*, vol. 9, pp. 24273–24287, 2021, doi: 10.1109/ACCESS.2021.3056516.
- [2] M. Desai and M. Shah, "An anatomization on breast cancer detection and diagnosis employing multi-layer perceptron neural network (MLP) and Convolutional neural network (CNN)," *Clin. EHealth*, vol. 4, pp. 1–11, 2021, doi: 10.1016/j.ceh.2020.11.002.
- [3] G. Hamed, M. Marey, S. E. Amin, and M. F. Tolba, "Automated Breast Cancer Detection and Classification in Full Field Digital Mammograms Using Two Full and Cropped Detection Paths Approach," *IEEE Access*, vol. 9, pp. 116898–116913, 2021, doi: 10.1109/ACCESS.2021.3105924.
- [4] F. F. Ting, Y. J. Tan, and K. S. Sim, "Convolutional neural network improvement for breast cancer classification," *Expert Syst. Appl.*, vol. 120, pp. 103–115, Apr. 2019, doi: 10.1016/j.eswa.2018.11.008.
- [5] H. Aljuaid, N. Alturki, N. Alsubaie, L. Cavallaro, and A. Liotta, "Computer-aided diagnosis for breast cancer classification using deep neural networks and transfer learning," *Comput. Methods Programs Biomed.*, vol. 223, p. 106951, Aug. 2022, doi: 10.1016/j.cmpb.2022.106951.
- [6] A. Chetlen, J. Mack, and T. Chan, "Breast cancer screening controversies: who, when, why, and how?," *Clin. Imaging*, vol. 40, no. 2, pp. 279–282, Mar. 2016, doi: 10.1016/j.clinimag.2015.05.017.
- [7] Y. M. George, H. H. Zayed, M. I. Roushdy, and B. M. Elbagoury, "Remote Computer-Aided Breast Cancer Detection and Diagnosis System Based on Cytological Images," *IEEE Syst. J.*, vol. 8, no. 3, pp. 949–964, Sep. 2014, doi: 10.1109/JYST.2013.2279415.
- [8] M. T. McCann, J. A. Ozolek, C. A. Castro, B. Parvin, and J. Kovacevic, "Automated Histology Analysis: Opportunities for signal processing," *IEEE Signal Process. Mag.*, vol. 32, no. 1, pp. 78–87, Jan. 2015, doi:

10.1109/MSP.2014.2346443.

- [9] A. Sahu, P. K. Das, and S. Meher, "An efficient deep learning scheme to detect breast cancer using mammogram and ultrasound breast images," *Biomed. Signal Process. Control*, vol. 87, p. 105377, Jan. 2024, doi: 10.1016/j.bspc.2023.105377.
- [10] H. Lee, J. Park, and J. Y. Hwang, "Channel Attention Module with Multi-scale Grid Average Pooling for Breast Cancer Segmentation in an Ultrasound Image," *IEEE Trans. Ultrason. Ferroelectr. Freq. Control*, pp. 1–1, 2020, doi: 10.1109/TUFFC.2020.2972573.
- [11] M. Toğaçar, K. B. Özkurt, B. Ergen, and Z. Cömert, "BreastNet: A novel convolutional neural network model through histopathological images for the diagnosis of breast cancer," *Phys. Stat. Mech. Its Appl.*, vol. 545, p. 123592, May 2020, doi: 10.1016/j.physa.2019.123592.
- [12] S. Jiang and V. Zavala, "Convolutional Neural Nets in Chemical Engineering: Foundations, Computations, and Applications," *AIChE J.*, vol. 67, May 2021, doi: 10.1002/aic.17282.
- [13] S. Albawi, T. A. Mohammed, and S. Al-Zawi, "Understanding of a convolutional neural network," in *2017 International Conference on Engineering and Technology (ICET)*, Aug. 2017, pp. 1–6. doi: 10.1109/ICEngTechnol.2017.8308186.
- [14] J. Schmidhuber, "Deep learning in neural networks: An overview," *Neural Netw.*, vol. 61, pp. 85–117, Jan. 2015, doi: 10.1016/j.neunet.2014.09.003.
- [15] J. Xu, Z. Li, B. Du, M. Zhang, and J. Liu, "Reluplex made more practical: Leaky ReLU".
- [16] K. He, X. Zhang, S. Ren, and J. Sun, "Delving Deep into Rectifiers: Surpassing Human-Level Performance on ImageNet Classification," in *2015 IEEE International Conference on Computer Vision (ICCV)*, Santiago, Chile: IEEE, Dec. 2015, pp. 1026–1034. doi: 10.1109/ICCV.2015.123.
- [17] H. Wang, S. Xu, K. Fang, Z.-S. Dai, G.-Z. Wei, and L.-F. Chen, "Contrast-enhanced magnetic resonance image segmentation based on

- improved U-Net and Inception-ResNet in the diagnosis of spinal metastases,” *J. Bone Oncol.*, vol. 42, p. 100498, Oct. 2023, doi: 10.1016/j.jbo.2023.100498.
- [18] I. U. Haq, H. Ali, H. Y. Wang, C. Lei, and H. Ali, “Feature fusion and Ensemble learning-based CNN model for mammographic image classification,” *J. King Saud Univ. - Comput. Inf. Sci.*, vol. 34, no. 6, pp. 3310–3318, Jun. 2022, doi: 10.1016/j.jksuci.2022.03.023.
- [19] Y. Liang and Z. Meng, “Brea-Net: An Interpretable Dual-Attention Network for Imbalanced Breast Cancer Classification,” *IEEE Access*, vol. 11, pp. 100508–100517, 2023, doi: 10.1109/ACCESS.2023.3314978.
- [20] E. Alkhaldi and E. Salari, “Ensemble Optimization for Invasive Ductal Carcinoma (IDC) Classification Using Differential Cartesian Genetic Programming,” *IEEE Access*, vol. 10, pp. 128790–128799, 2022, doi: 10.1109/ACCESS.2022.3228176.
- [21] B. Xu *et al.*, “Attention by Selection: A Deep Selective Attention Approach to Breast Cancer Classification,” *IEEE Trans. Med. Imaging*, vol. 39, no. 6, pp. 1930–1941, Jun. 2020, doi: 10.1109/TMI.2019.2962013.
- [22] N. Wu *et al.*, “Deep Neural Networks Improve Radiologists’ Performance in Breast Cancer Screening,” *IEEE Trans. Med. Imaging*, vol. 39, no. 4, pp. 1184–1194, Apr. 2020, doi: 10.1109/TMI.2019.2945514.
- [23] H. Chougrad, H. Zouaki, and O. Alheyane, “Deep Convolutional Neural Networks for breast cancer screening,” *Comput. Methods Programs Biomed.*, vol. 157, pp. 19–30, Apr. 2018, doi: 10.1016/j.cmpb.2018.01.011.
- [24] X. Yu, C. Kang, D. S. Guttery, S. Kadry, Y. Chen, and Y.-D. Zhang, “ResNet-SCDA-50 for Breast Abnormality Classification,” *IEEE/ACM Trans. Comput. Biol. Bioinform.*, vol. 18, no. 1, pp. 94–102, Jan. 2021, doi: 10.1109/TCBB.2020.2986544.
- [25] N. Arya and S. Saha, “Multi-modal classification for human breast cancer prognosis prediction: Proposal of deep-learning based stacked ensemble model,” *IEEE/ACM Trans. Comput. Biol. Bioinform.*, pp. 1–1, 2020, doi: 10.1109/TCBB.2020.3018467.

- [26] S. Chattopadhyay, A. Dey, P. K. Singh, D. Oliva, E. Cuevas, and R. Sarkar, "MTRRE-Net: A deep learning model for detection of breast cancer from histopathological images," *Comput. Biol. Med.*, vol. 150, p. 106155, Nov. 2022, doi: 10.1016/j.combiomed.2022.106155.
- [27] D. Addo *et al.*, "A hybrid lightweight breast cancer classification framework using the histopathological images," *Biocybern. Biomed. Eng.*, vol. 44, no. 1, pp. 31–54, Jan. 2024, doi: 10.1016/j.bbe.2023.12.003.
- [28] R. Athilakshmi, R. Jansi, and R. Upadhyay, "Enhancing Diabetic Retinopathy Diagnosis with Inception v4: A Deep Learning Approach," in *2023 5th International Conference on Inventive Research in Computing Applications (ICIRCA)*, Coimbatore, India: IEEE, Aug. 2023, pp. 905–910. doi: 10.1109/ICIRCA57980.2023.10220890.
- [29] C. Szegedy, S. Ioffe, V. Vanhoucke, and A. Alemi, "Inception-v4, Inception-ResNet and the Impact of Residual Connections on Learning." arXiv, Aug. 23, 2016. Accessed: Mar. 12, 2024. [Online]. Available: <http://arxiv.org/abs/1602.07261>
- [30] Y. Wang, Z. Yang, S. Ren, X. Gouliu, J. Gao, and T. Wang, "DDRSNet-Rail Surface Defects Classification Based on Depthwise-Dilated Convolution," in *2023 International Conference on Image Processing, Computer Vision and Machine Learning (ICICML)*, Nov. 2023, pp. 721–724. doi: 10.1109/ICICML60161.2023.10424928.
- [31] Y. Jiang, Z. Huang, L. Li, and Q. Dong, "Local–global dual attention network (LGANet) for population estimation using remote sensing imagery," *Resour. Environ. Sustain.*, vol. 14, p. 100136, Dec. 2023, doi: 10.1016/j.resenv.2023.100136.
- [32] A. Wanto, Y. Yuhandri, and O. Okfalisa, "Optimization Accuracy of CNN Model by Utilizing CLAHE Parameters in Image Classification Problems," in *2023 International Conference on Networking, Electrical Engineering, Computer Science, and Technology (IConNECT)*, Bandar Lampung, Indonesia: IEEE, Aug. 2023, pp. 253–258. doi: 10.1109/IConNECT56593.2023.10327100.

- [33] C. Wang, X. Miao, Y. Xi, M. Bi, L. Li, and W. Hu, “Interpretable and visualized SHAP-based equalizer with feature selection in IMDD system,” in *Optical Fiber Communication Conference (OFC) 2021*, Washington, DC: Optica Publishing Group, 2021, p. Th1A.1. doi: 10.1364/OFC.2021.Th1A.1.
- [34] T. He *et al.*, “MediMLP: Using Grad-CAM to Extract Crucial Variables for Lung Cancer Postoperative Complication Prediction,” *IEEE J. Biomed. Health Inform.*, vol. 24, no. 6, pp. 1762–1771, Jun. 2020, doi: 10.1109/JBHI.2019.2949601.

Appendices

The project is on Github, URL is as follow:

https://github.com/Vio1etV/Final_Year_Project

The dataset link:

[BreakHis \(kaggle.com\)](#)